Pure Appl. Geophys.
© 2022 The Author(s), under exclusive licence to Springer Nature Switzerland AG
https://doi.org/10.1007/s00024-022-02994-1

Pure and Applied Geophysics

A New Insight into the Structural Framework of a Crystalline Formation and the Adjoining Sedimentary Terrain in Parts of the Precambrian Basement Complex of Nigeria

Leke Sunday Adebiyi,[1,2] Akinola Bolaji Eluwole,[2] Naheem Banji Salawu,[2,3] Sesan Cornelius Falade,[1] Kehinde Oladele Dopamu,[1] and Esther Adetola Alejolowo[1]

Abstract—The present study investigates geological structures in parts of the crystalline basement and the adjoining middle Niger Basin of Nigeria using high-resolution airborne magnetic and radiometric data. The purpose is to provide additional insights into the contrasting structures of the magnetic basement within the crystalline and the sedimentary terrain. The magnetic and radiometric data of the study area were subjected to standard interpretation techniques. The results obtained showed the entire crystalline basement to be overprinted by younger igneous rocks at extremely shallow depths. The sedimentary basin on the other hand is marked by basement subsidence and volcanic intrusions. Two major shear zones traverse the crystalline basement and the adjoining sedimentary basin. The shear zones cross-cut the entire study area in a NNE direction and exhibit three major dipping contacts, namely, vertical-, north-western- and south-eastern-dipping contacts in specific locations. The shear zones exhibit multiple surface faults mostly within the crystalline basement and are characterized by linear magnetic highs that indicate magnetic minerals precipitate in specific areas. Some parts are characterized by a low-amplitude magnetic anomaly that coincides with high potassium and fairly low thorium concentrations that indicate the presence of younger volcanic rocks and possibly gold mineralization in the shear planes. The zones are parallel to the trans-current Ifewara–Kalangai–Zungeru shear zone already linked to the South Atlantic transform fault system. The structural architecture of the study area and perhaps the entire basement complex displayed a positive prospect for economic minerals in specific locations.

Keywords: Radiometric method, magnetic method, mineral deposits, crystalline basement, sedimentary basin.

1. Introduction

The Nigerian formation is made up of the exposed crystalline basement and the sedimentary basins. The exposed crystalline basement occupies three parts, namely the south-western, south-eastern and north-central half of Nigeria, while the sedimentary basins unconformably overlie the crystalline basement in the Benue Trough, middle Niger Basin, Sokoto Basin, Chad Basin, Dahomey Basin and the Niger Delta Basin—which is a prolongation of the Atlantic sediments (Adebiyi et al., 2020; Haruna, 2017; Odeyemi, 1976; Oluyide, 1988; Rahaman, 1976). The crystalline basement of Nigeria is lithologically divergent. This gives credit to the general understanding that the earth crust is made up of structures and rocks of extensively diverse ages. The presence of several prominent structures such as the shear zones, fold belts among others in Nigeria and other orogenic provinces showed that plate tectonics is significant in the development of continental crust (Alessio et al., 2017; Dada, 1998; Grant, 1969, 1978; Wright et al., 1985). The study area is part of the Precambrian basement complex of Nigeria. It is overlain by the crystalline rocks in the western part and by cretaceous sediments in the eastern part. The transition from crystalline basement in the western part to the sedimentary basin in the eastern part presents the main structural complexity for the exploration of the recognized mineral deposits in the study area. The map of Africa (Fig. 1a) shows the location of Nigeria in West Africa. The map highlights two major rivers in Nigeria, namely the Niger and Benue rivers. The study area lies between the present Kwara and Niger States (Fig. 1b) and is

[1] Department of Physical Sciences, Landmark University, PMB 1001, Omu-Aran, Kwara State, Nigeria. E-mail: adebiyi.leke@lmu.edu.ng; olalakes2012@gmail.com

[2] Department of Geophysics, Federal University, Oye Ekiti, Ekiti State, Nigeria.

[3] BS Geophysical and Consultancy Ltd., Ilorin, Nigeria.

Published online: 18 March 2022

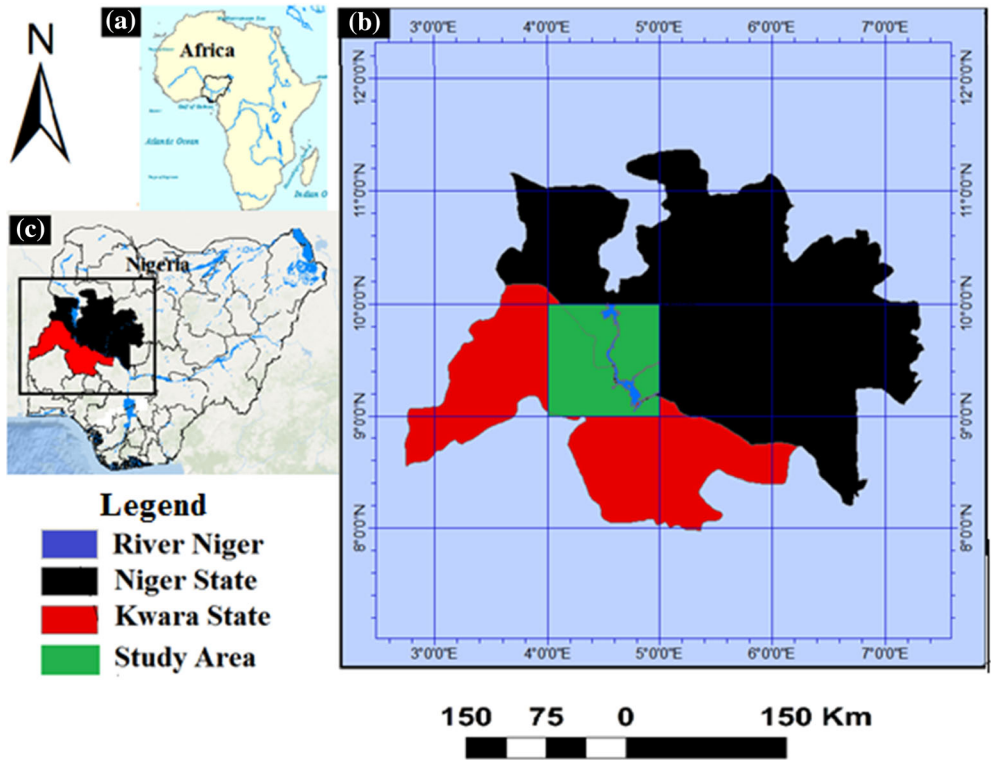

Figure 1
a Map of Africa showing the location of Nigeria in West Africa; **b** political map of Nigeria showing the present Kwara and the Niger states; **c** location map showing the study area (green) between the present Kwara (red area) and the Niger (black area) states

highlighted in green in Fig. 1c. It extends from longitude 4° 00′ 00″ E to 5° 00′ 00″ E, and latitude 9° 00′ 00″ N to 10° 00′ 00″ N, covering approximately 48,400 km^2 on land. It is drained mainly by the Niger River and minor tributaries (highlighted in blue on the map). The mining activities in the area involve indiscriminate excavation of suspected mineralized structures in parts of Jebba, Kainji, Sabongida and Borgu, among others. The general geology of the area shows primarily the crystalline basement rocks of west-central Nigeria and are contiguous with the middle Niger Basin in the eastern study area. The study area and most parts of the Nigerian basement complex are presumably rich in minerals such as gold, lead, tin and copper. However, the lack of sufficient information as regards the structural disposition of many areas has affected the choice of exploration of many of the minerals. This is further complicated by rugged and fairly inaccessible terrain that hinders ground surveys. The present study aims to provide new insights into the geological framework of the study area through the recognition of appropriate structures that will further guide the exploration of economic minerals in the area. To achieve this, we carried out both qualitative and quantitative interpretation of high-resolution aeromagnetic data using standard geophysical tools such as the first-order vertical derivative, total gradient magnitude, horizontal gradient magnitude, Euler deconvolution and source parameter imaging. We equally interpreted airborne radiometric data to complement the aeromagnetic data. We present simplified two-dimensional (2D) sections of the subsurface morphology from the interpreted maps to aid the visual interpretation of notable geological structures in the study area. The study, in general, is based on the effectiveness of the magnetic data in delineating the location, strikes, dip, shape, lateral and depth extent of subsurface structures and in sedimentary basins for estimating sedimentary

thickness and mapping of volcanic intrusions (Nabighian et al., 2005). The study equally utilized the complementary power of the radiometric data regarding the delineation of chemical alteration in rocks and structures of tectonic origin (Gunn et al., 1997).

2. Geological Setting

2.1. The Crystalline Basement

The crystalline basement rocks that form the study area display a poly-orogenic sequence of a reworked Archaean migmatite–gneiss complex comprising mainly granite gneiss, migmatite, medium- to coarse-grained biotite and hornblende granite, and minor fine-grained flaggy quartz-biotite gneiss, porphyritic granite, undifferentiated schist with banded gneiss, quartz schist, and fine-grained biotite granite (Fig. 2). It is part of the Precambrian basement complex that lies within the Trans-Sahara mobile belt between the West African Craton, the Gabon-Congo Craton and the Sahara meta-craton within the framework of the late Proterozoic and early Paleozoic Gondwana amalgam (Adebiyi et al., 2021; Ajibade et al., 1987; Dada, 2008; Salawu, Fatoba, et al., 2020). The crystalline basement and the adjoining middle Niger Basin have been identified with a NNE-trending transcurrent Ifewara–Kalangai–Zungeru shear zone with a link to the South Atlantic transform fault system (Adepelumi et al., 2008; Anifowose et al., 2010; Awoyemi, Ajama, et al., 2017; Awoyemi, Hammed, et al., 2017; Odeyemi et al., 1999; Salawu, Fatoba, et al., 2020; Udensi et al., 2003). This mega-structural shear zone has been recognized as a possible crustal suture at the time of the Pan-African orogeny (Ajibade & Wright, 1988; Awoyemi, Hammed, et al., 2017; Awoyemi, Ajama, et al., 2017; Dada, 2008; Garba, 2000; McCurry & Wright, 1977; Salawu, Fatoba, et al., 2020; Wright et al., 1985).

2.2. The Sedimentary Terrain

The sedimentary terrain is part of the middle Niger Basin (See Fig. 2). The basin is presumably a north-western extension of the Anambra Basin and is subdivided into the northern and the southern arms (Kogbe, 1989; Rahaman et al., 2018). The portion of the middle Niger Basin that formed part of the present study area falls within the northern part and has mainly the Sakpe formation. The basin fills consist of a NW-trending belt of Upper Cretaceous (Campano-Maastrichtian) sediments which resulted from rifting, basement fragmentation, block faulting, drifting subsidence, and deposition of the latter material and subsequent opening of the South Atlantic Ocean (Obaje, 2009; Salawu, Fatoba, et al., 2020). Several studies conducted in many parts of the basin uphold the observation that the basin was, perhaps, a product of rifting. A study by Kogbe (1981) involving the interpretation of geophysical data, Landsat images and borehole logs identified structures typical of a rift basin. Similar studies by Kogbe et al. (1983) and Ojo and Ajakaiye (1989) using gravity data linked the basin evolution to a rift. However, the maximum depth for the various parts of the basin has been the centre of many discussions for years. Earlier studies suggest depth values between 3.4 and 6.1 km (Adeniyi, 1985; Ojo, 1984, 1990; Olaniyi et al., 2012; Udensi & Osazuwa, 2004), while the more recent studies suggest maximum depth values of not more than 1 km (Megwara & Udensi, 2014; Salawu, Fatoba, et al., 2020). Also forming an important part of the discussions is the observation that the basin has no volcanic intrusion within the sedimentary unit (Kogbe, 1989; Ojo & Ajakaiye, 1989; Rahaman et al., 2018). The volcanic intrusions are believed to be restricted within the basement (Ojo & Ajakaiye, 1989; Whiteman, 1982).

3. Data

3.1. Topography Data

The topography data in this study is the remotely sensed Shuttle Radar Topographic Mission (SRTM) digital elevation model (DEM) downloaded from the website of the United States Geological Survey (USGS, 2017). The original data was converted from raster to grid to help visualize subtle variation in the topography of the study area (see Fig. 3). The DEM

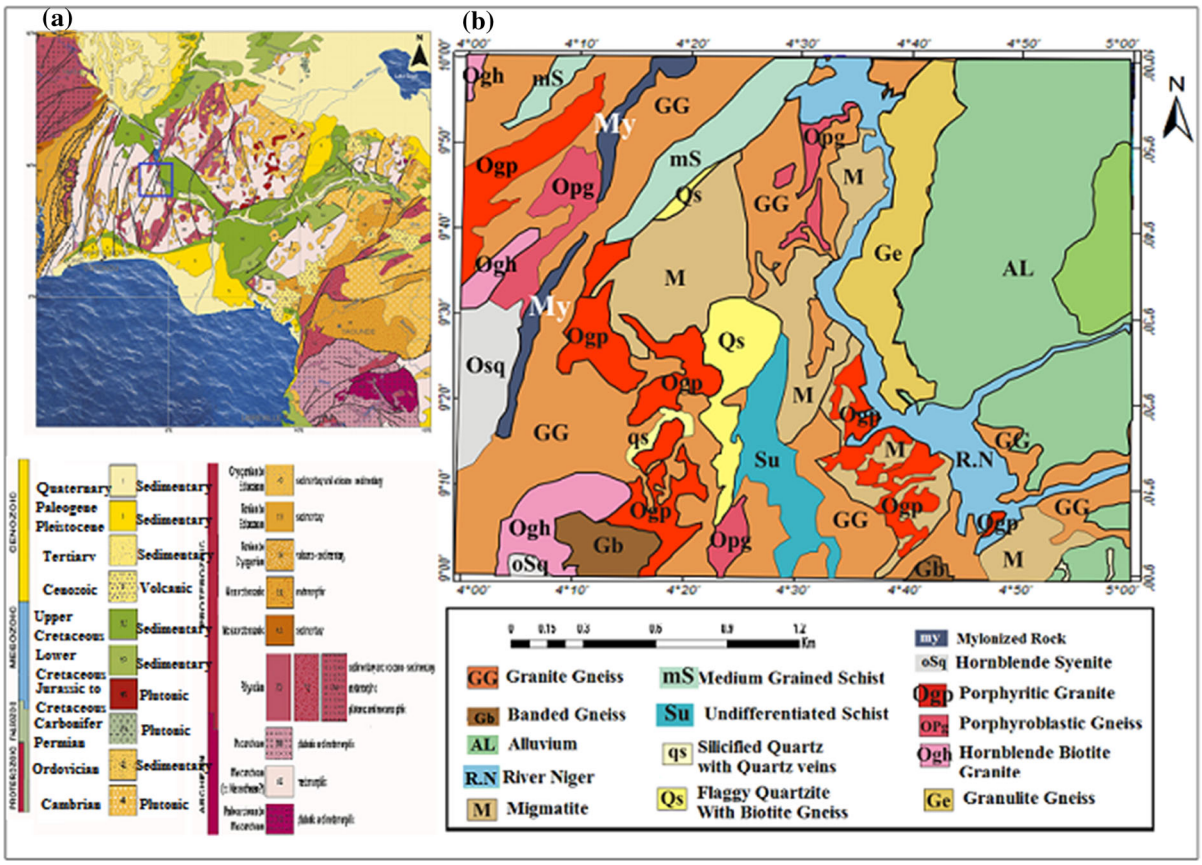

Figure 2
a Simplified geology map of Nigeria and environs showing the study location (Salawu, Fatoba, et al., 2020; Salawu, Orosun, et al., 2020; Thieblemont, 2016); **b** geology map of the study area (NGSA, 2006a)

with the airborne magnetic data was used for the elevation correction on the 2D subsurface models. The traverses and directions of four cross sections A–A′, B–B′, C–C′ and D–D′ used for the subsurface models are shown on the DEM map (Fig. 3). We identified on the map two suspected mega-structural fractures through the study area (shown as white broken lines). Similarly, the boundary of the crystalline basement and the sedimentary terrain was identified with a yellow broken line. The DEM map (Fig. 3) shows the course of the Niger River through the study area. The river flows southward from the north through a narrow path that is surrounded on both sides by hard crystalline rocks that rise abruptly above the river mean elevation. The crystalline basement on the western part of the study area has an elevation almost everywhere above 300 m, while the sedimentary terrain on the eastern study area has elevation measuring up to 280 m only in specific areas. One interesting topographic feature is the overall partitioning of the study area into the western crystalline basement and the eastern sedimentary terrain by the Niger River.

3.2. *Magnetic Data*

Magnetic data used consist of four half-degree sheets of high-resolution aeromagnetic data provided by the Nigerian Geological Survey Agency (NGSA). The data formed part of the regional high-resolution airborne data of Nigeria acquired by Fugro Airborne Surveys on a series of NW–SE trends (NGSA, 2006b). The flight line and tie-line spacing used to acquire the data were 500 m and 2000 m,

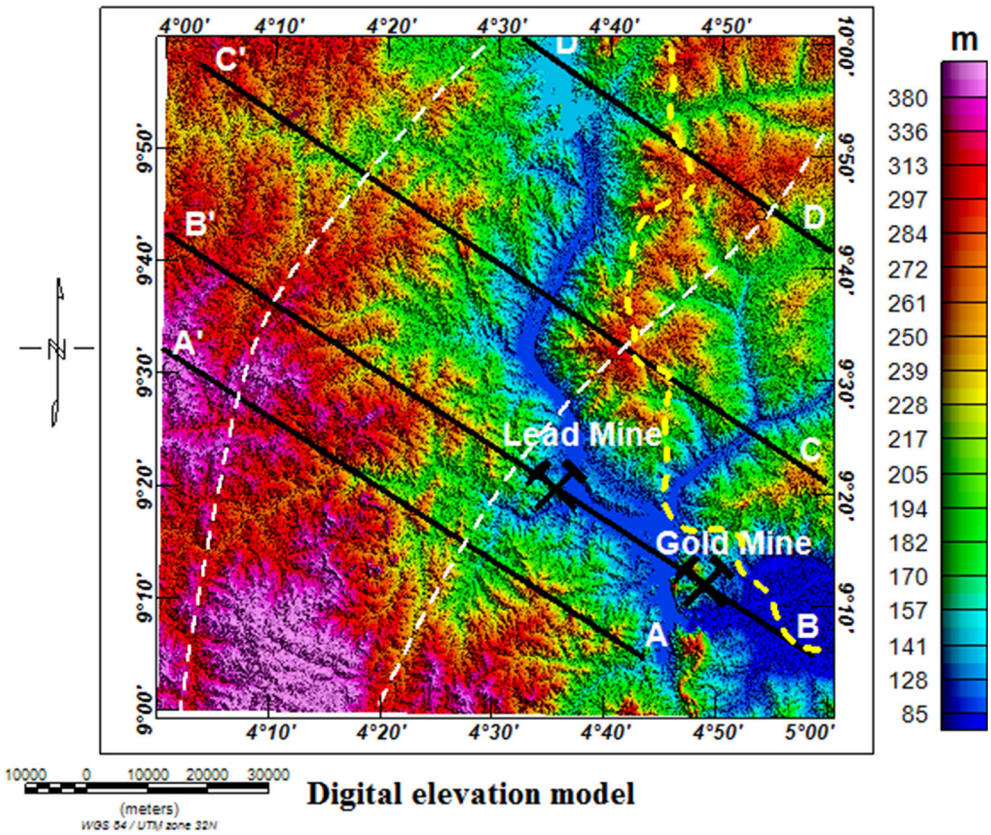

Figure 3
Colour-shaded digital elevation model data of the study area. The map highlights four NW–SE 2D cross-sections A–A′, B–B′, C–C′ and D–D′ cutting across important geological structures and suspected faults. The cross section B–B′ has two active mining sites where gold and lead minerals are mined. The white broken lines represent the position of the shear zones through the study area. The boundary of the middle Niger Basin to the east and the crystalline basement to the west is also outlined in a yellow broken line

respectively, at an average barometric flight height of about 80 m. Necessary corrections including the removal of the international geomagnetic reference field (IGRF) from the magnetic data were carried out by Fugro Airborne Surveys. The resulting data were gridded at 100-m spacing using the minimum curvature gridding algorithm (Brigs, 1974) and displayed as a 2D residual magnetic intensity (RMI) map (see Fig. 4). Four NW-trending cross sections, A–A′, B–B′, C–C′ and D–D′ (black lines), were used to display the 2D cross sections of the subsurface structures within the crystalline basement and the adjoining sedimentary terrain. The cross section B–B′ passes through two known mining sites to provide additional insights into the mineral prospect in the mining sites. A yellow broken line in Fig. 4 is equally used to show the boundary of the sedimentary basin and the crystalline basement. Similarly, the strike and linear extent of two suspected shear zones through the study area is shown in white broken lines.

3.3. Radiometric Data

Radiometric data in this study consist of four half-degree sheets of airborne radiometric data acquired at the same time as the airborne magnetic data by mounting a high-precision gamma-ray spectrometer with the aircraft that also carried a proton-precession magnetometer (NGSA, 2006b). The original data were corrected for background radiation and other necessary corrections by Fugro Airborne Surveys Company. The resulting data were gridded at 100-m

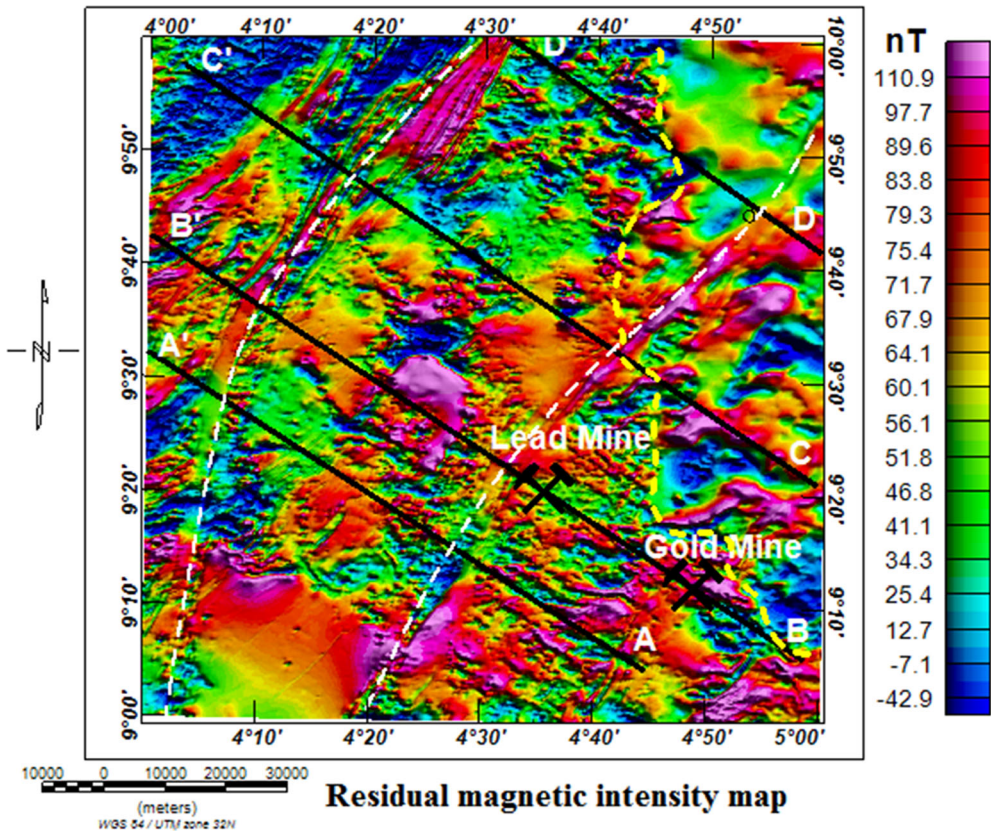

Figure 4
Colour-shaded residual magnetic intensity (RMI) map over the study area. The map highlights four NW–SE 2D cross sections, A–A′, B–B′, C–C′ and D–D′, cutting across important geological structures and suspected faults. The white broken lines represent the position of the shear zones through the study area. The boundary of the middle Niger Basin to the east and the crystalline basement to the west is also outlined in yellow

spacing using the minimum curvature gridding algorithm (Brigs, 1974) and displayed as radiometric grids comprising potassium (K), thorium (eTh) and uranium (eU). The radiometric grids were converted to maps and presented as Fig. 5a–c, respectively. The sedimentary segment of the study area shows exceptionally low potassium concentration (Fig. 5a) and fairly low thorium and uranium concentration (Fig. 5b, c). The crystalline basement, on the other hand, is characterized by fairly low to high radiometric concentration. Very large parts of the crystalline basement displayed potassium concentration as high as 4.1%. Similarly, thorium and uranium concentrations in many parts of the crystalline basement are as high as 27.1 ppm and 5.9 ppm, respectively. The radiometric concentration maps equally highlighted the Niger river course through the study area.

4. Method

4.1. Magnetic Methods

Interpreting magnetic data in the present study area and perhaps several other locations in Nigeria is exceptionally complex because of the proximity to the magnetic equator. The magnetic equator through Nigeria is well documented (Akingboye & Ogunleye, 2018) where it seemingly divides the country into three magnetic belts such that some locations lie on the equator, while other locations lie north and south of the equator. To effectively carry out the

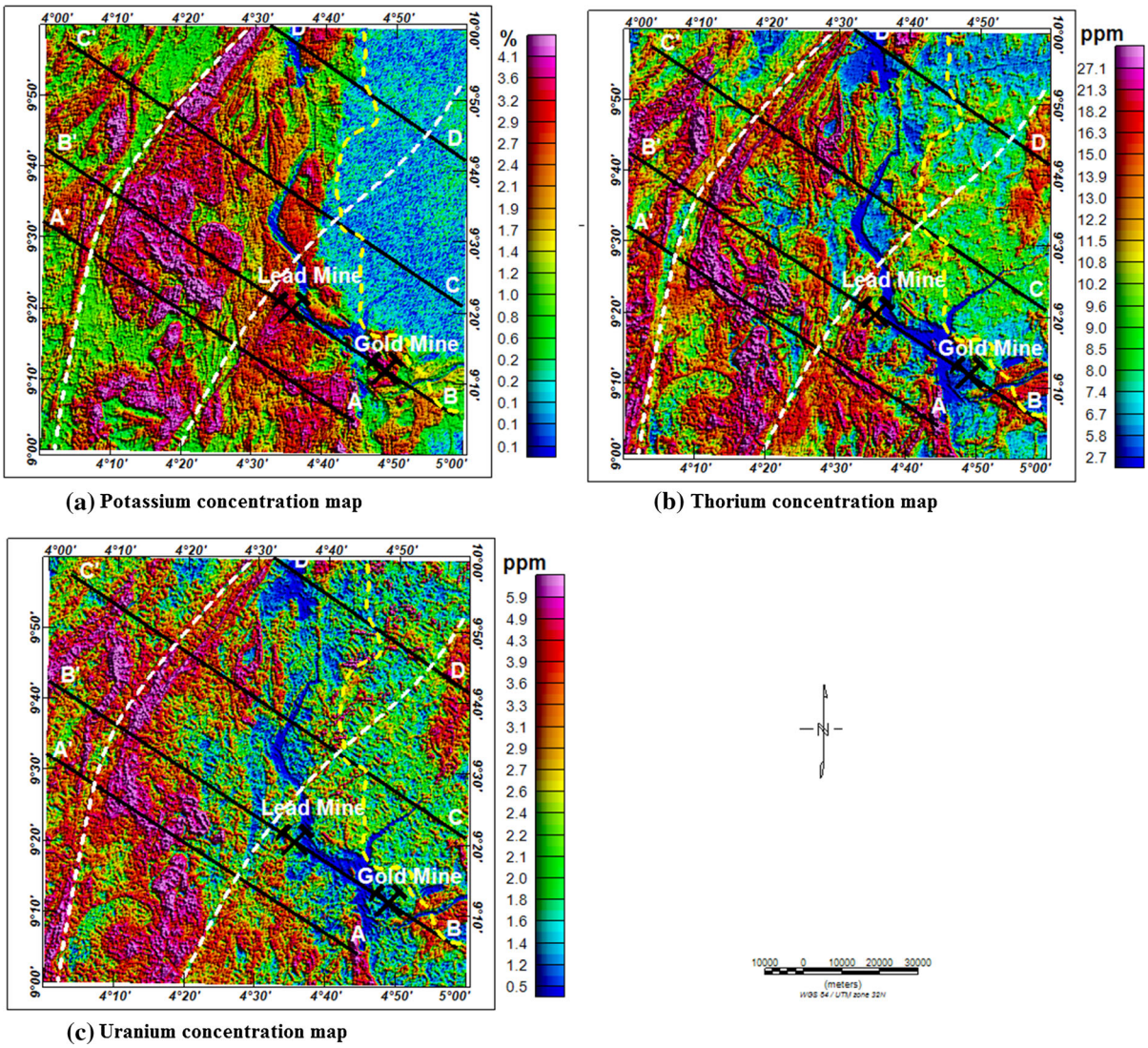

Figure 5
a Potassium concentration map; **b** thorium concentration map; **c** uranium concentration map. The locations of the mines are shown on profile B–B′

interpretation of the magnetic data in Nigeria, the understanding of the location of the study area relative to the magnetic equator at the time of the data acquisition is very paramountt. This gives the interpreter an idea of the magnetic field direction in the survey area. The magnetic field in the present study area, at the time of the survey, was inclined at –4.4° (NGSA, 2006b). The acquired data were interpreted using the first-order vertical derivative (FVD), total gradient magnitude (TGM), horizontal gradient magnitude (HGM), three-dimensional (3D) Euler deconvolution and source parameter imaging (SPI). The various methods used are notably complementary since all methods have their weaknesses.

4.1.1 First-Order Vertical Derivative

The first-order vertical derivative (FVD) is often applied to magnetic data to interpret shallow-seated magnetic structures and rocks such as geological

contacts, fractures, volcanic intrusions, mineral porphyry among others (Nabighian et al., 2005). Interpretation of the FVD map is wholly qualitative and involves visual inspection of linear and isolated magnetic anomalies on the map. The result is independent of magnetic inclination and therefore able to detect, very precisely, several shallow-seated magnetic source bodies. Equation 1 shows the first-order vertical derivative of the residual magnetic intensity F.

$$FVD = \frac{dF}{dz} \tag{1}$$

4.1.2 Total Gradient Magnitude Interpretation

Total gradient magnitude (TGM) is effective for interpreting magnetic data for 2D source bodies. The method, for 3D magnetic source bodies, is sensitive to the direction of magnetization, magnetic remanence, dip angle, top and bottom depths of magnetic source bodies (Huang & Guan, 1998; Li, 2006). Barring the aforementioned limitations, the TGM is an excellent qualitative method for visual inspection of a magnetic anomaly (MacLeod et al., 1993). Furthermore, an offset of the horizontal gradient magnitude (HGM) maxima from the TGM maxima is used to infer the dip direction of the magnetic structure (Philip, 2000; Awoyemi, Ajama, et al., 2017). Equation 2 shows the expression for TGM interpretation for gridded magnetic data.

$$|TGM(x,y)| = \sqrt{\left(\frac{\partial F}{\partial x}\right)^2 + \left(\frac{\partial F}{\partial y}\right)^2 + \left(\frac{\partial F}{\partial z}\right)^2} \tag{2}$$

where $\frac{\partial F}{\partial x}$ and $\frac{\partial F}{\partial y}$ are the first-order partial derivatives of the residual magnetic intensity field, F in x and y horizontal directions, respectively, while $\frac{\partial F}{\partial z}$ is the first-order partial derivative of the residual magnetic intensity field,F in a z vertical direction. Further information relating to TGM interpretation is available in the published works of Verduzco et al. (2004) and Nabighian (1972), while a modified version is contained in the published work of Li (2006). Application of TGM interpretation to geological data is available in the published works of Adebiyi et al. (2020), Salawu, Orosun, et al. (2020) and Salawu et al. (2019).

4.1.3 Horizontal Gradient Magnitude Interpretation

The horizontal gradient magnitude (HGM) method involves finding the magnitude of the first-order horizontal derivatives of the field (Cordell & Grauch, 1982). To implement HGM interpretation, the expression in Eq. 3 is applied to magnetic data that has been corrected for diurnal variation, the international geomagnetic reference field (IGRF) and, where applicable, reduced to the magnetic equator or pole.

$$|HGM(x,y)| = \sqrt{\left(\frac{\partial F}{\partial x}\right)^2 + \left(\frac{\partial F}{\partial y}\right)^2} \tag{3}$$

where $\frac{\partial F}{\partial x}$ and $\frac{\partial F}{\partial y}$ are the first-order partial derivatives of the residual magnetic intensity field, F in x and y horizontal directions, respectively (Cordell & Grauch, 1982). The method can be used as an approximation of the total gradient magnitude over a non-dipping contact for zero inclination and declination (Awoyemi, Ajama, et al., 2017). The method is used, generally, to detect linear structures such as contacts and faults from potential field data. This is based on the assumptions that the magnetic field and source magnetization are vertical, the contact is vertical and the sources are thick (Philips, 2000). To satisfy the first two assumptions, it is necessary to apply a standard phase shift to the data known as a reduction to the equator for low-latitude magnetic data or to the pole for high-latitude magnetic data using a Fourier transform. Provided that the assumptions are satisfied, the method is effective in mapping lineaments that may correspond to basement faults and contacts. The HGM method is less susceptible to noise in the data (Fedi & Florio, 2001; Moritz, 2009) and, therefore, very reliable for interpreting low-latitude magnetic data, especially, the equatorial data.

4.1.4 Three-Dimensional Euler Deconvolution Interpretation

Three-dimensional Euler deconvolution is a quantitative method used mainly for interpreting magnetic data. It is used for interpreting the depths and shapes of idealized magnetic source bodies such as contacts, dykes, sills, vertical pipes, horizontal cylinders and spheres (Reid et al., 1990; Thompson, 1982). It can

also be used to estimate the horizontal position of the source and the base level at which the magnetic anomaly lies. Three-dimensional Euler deconvolution requires correct estimation of the structural index but does not require magnetic data to be corrected for a regional field. The method exploits a moving window and calculates the first-order derivatives of x, y and z (Eq. 4).

$$(x - x_0)\frac{\partial F}{\partial x} + (y - y_0)\frac{\partial F}{\partial y} + (z - z_0)\frac{\partial F}{\partial z} = N(B - F) \tag{4}$$

where F is the total field, B is the background level, (x, y, z) is the observation point, (x_0, y_0, z_0) is the source location and N is the structural index. $(\frac{\partial F}{\partial x})$, $(\frac{\partial F}{\partial y})$, $(\frac{\partial F}{\partial z})$ are the partial derivatives of F in the x, y and z directions, respectively. N is the structural index that generally assumes the values 0.0, 1.0, 2.0 and 3.0 to locate and calculate depths of magnetic contacts, dikes/sills, vertical pipes/horizontal cylinders and spheres, respectively (Reid et al., 1990, 2011). The method is not dependent on the magnetic field direction and so is highly effective for precisely mapping geological structures. Table 1 shows the structural indices of known geological models.

4.1.5 Source Parameter Imaging Interpretation

Source parameter imaging (SPI) interpretation often estimates depth values from the local wave number in Eq. 5 (Reid et al., 1990; Thurston & Smith, 1997a, 1997b).

Table 1

The magnetic structural index

Geological model	Number of infinite dimension	Magnetic structural index
Sphere	0	3.0
Pipe	1 (z)	2.0
Horizontal cylinder	1 (x – y)	2.0
Dyke	2 (z and x – y)	1.0
Sill	2 (x – y)	1.0
Contacts	3 (x, y, z)	0.0

$$K = \frac{\frac{\partial^2 F}{\partial x \partial z}\frac{\partial F}{\partial x} + \frac{\partial^2 F}{\partial y \partial z}\frac{\partial F}{\partial y} + \frac{\partial^2 F}{\partial z^2}\frac{\partial F}{\partial z}}{\left(\frac{\partial F}{\partial x}\right)^2 + \left(\frac{\partial F}{\partial y}\right)^2 + \left(\frac{\partial F}{\partial z}\right)^2} \tag{5}$$

where $K_{\max}$ is the maximum value of the local wave number (K) above the step-type source body. The depth estimates, therefore, are obtained from the reciprocal of the local wave number given in Eq. 6.

$$Depth_{x=0} = \frac{1}{K_{\max}} \tag{6}$$

The result obtained from the SPI interpretation is very reliable for estimating the depths to tops of 2D magnetic structures. The SPI depth map is very easy to analyse and often gives a good explanation of the subsurface topography.

4.2. Radiometric Method

The method of interpreting radiometric data is qualitative and involves finding the ratio of the channel data to obtain desirable features. The original data or the ratio maps can equally be combined to form a red–green–blue (RGB) ternary map.

4.2.1 Radiometric Ratios

The relative concentration of radio-elements in a given formation can be used as a benchmark for identifying different lithotypes and for identifying areas of preferential radio-element enrichment or depletion for mapping minerals precipitated in faults (Dentith & Mudge, 2014). For instance, a high potassium concentration accompanied by thorium depletion can be used to identify a shear zone where hydrothermal fluid accompanied the ejection of a volcano leading to hydrothermal alteration (Dentith & Mudge, 2014; Hafeez et al., 2015; Ohioma et al., 2017; Shives et al., 2000). This radiometric signature is often associated with linear and fairly broad magnetic lows (Gunn et al., 1997).

4.2.2 Ternary Radiometry Map of Principal Elements and Their Ratios

Another subtle way to visualize the relative abundance of radio-elements in a geological setting is to display, using an RGB colour combination, the

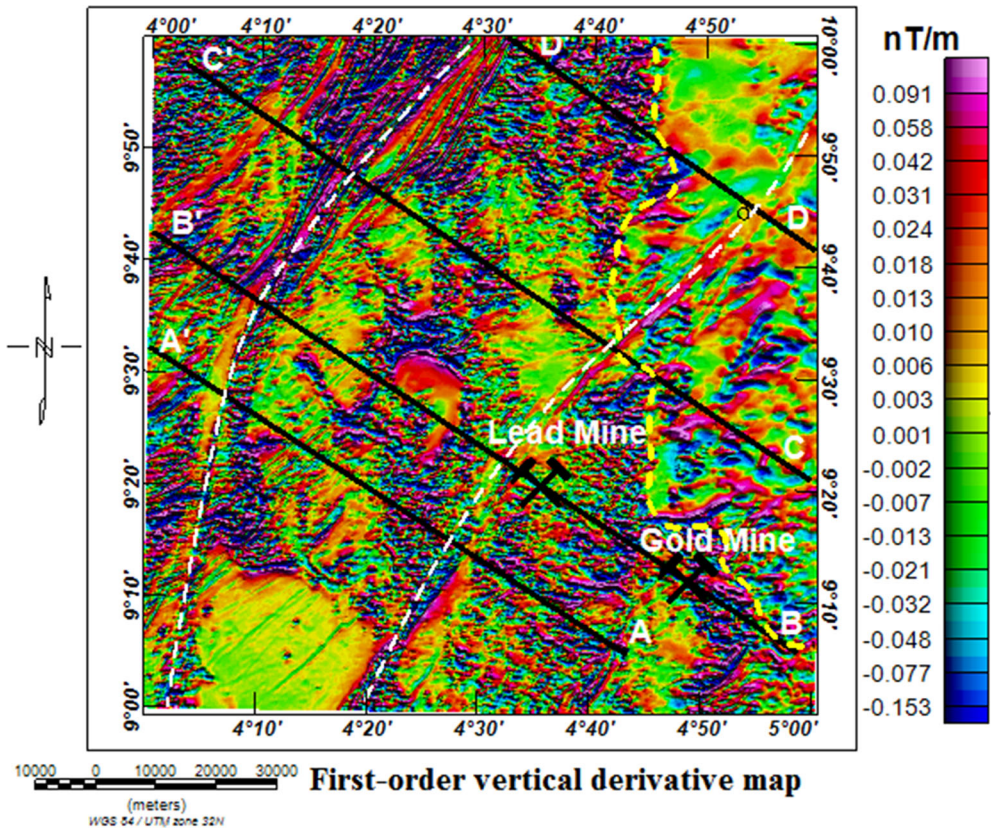

Figure 6
Colour-shaded map of the first-order vertical derivative. Four 2D cross sections on the map cut the major structures at fairly right angles. The shear zones through the study area have widths of several kilometres

principal element with its respective ratios such as K with K/eTh and K/eU, eTh with eTh/K and eTh/eU, and eU with eU/K and eU/eTh (Dentith & Mudge, 2014). Either way, the regions where the principal element is abundant appear white when the other radio-elements are low or appear red where both radio-elements have high concentrations (Dentith & Mudge, 2014). Areas where the three radio-elements have high concentrations appear red, while the parts depleted in the three radio-elements appear as cyan. Similar results will be obtained when the ternary radiometric maps of eTh, eTh/K, eTh/eU and eU, eU/K and eU/eTh were derived. However, the regions where thorium is slightly depleted compared to potassium and uranium often appear yellow. This can be used to identify mineral-bearing faults.

5. *Results and Discussion*

5.1. *First-Order Vertical Derivative*

The FVD filter was implemented to enhance shallow-seated magnetic intrusions and faults throughout the study area. The filter was implemented on the residual magnetic intensity data since it is not affected by inclination. The result obtained highlights numerous shallow-seated isolated magnetic bodies and a host of linear magnetic structures that can be interpreted as magnetic intrusions and faults, respectively (Fig. 6). Visual inspection of the map shows two prominent NNE-trending linear magnetic structures through the study area (highlighted as white broken lines on the maps). The strike length measured at different parts of the structures shows values greater than 5 km in specific locations.

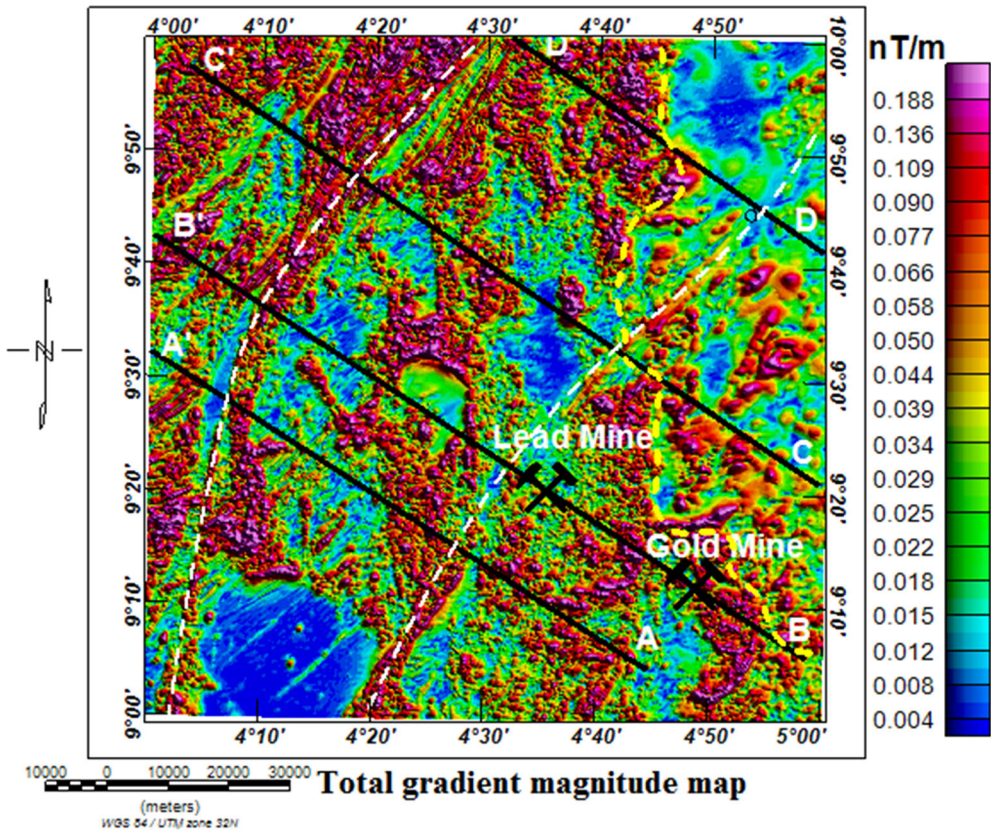

Figure 7
Colour-shaded total gradient magnitude (TGM) map of the study area. The map highlights magnetic structures throughout the study area

Ball (1980) and Thieblemont (2016) identified a few mega-structural faults in the crystalline basement complex of Nigeria and up to the boundary of the Dahomey Basin. Odeyemi et al. (1999), Adepelumi et al. (2008), Anifowose et al. (2010) and a host of others emphasized the possibility of a link between one of the faults known as the Ifewara–Kalangai–Zungeru trans-current fault and the South Atlantic transform fault system. However, the structures identified in the study area are not only mega-structural faults but also zones of intense mechanical shearing involving brittle surface and possibly internal ductile deformations. The shear zones show positive prospects for mineral exploration, though there is presently no active mining activity on the part through the study area. The result also highlights the boundary between the crystalline basement and the adjoining middle Niger Basin (shown as yellow broken lines on the maps). The basin shows pockets of magnetic anomalies, even though several previous studies identified it as a non-volcanic basin (Kogbe, 1989; Rahaman et al., 2018).

5.2. *Total Gradient Magnitude*

The TGM method was implemented to map mainly 2D magnetic source bodies and edges of linear magnetic structures such as the shear zones and other minor fractures in the study area. The method was implemented directly on the residual magnetic intensity dataset. The result obtained shows the distribution of the magnetic structures within the crystalline basement and the adjoining sedimentary terrain (Fig. 7). The map equally highlighted several minor fractures and the two shear zones. The shear zones are characterized by linear and fairly broad magnetic anomalies in specific locations. The magnetic anomalies, in different parts of the shear zones,

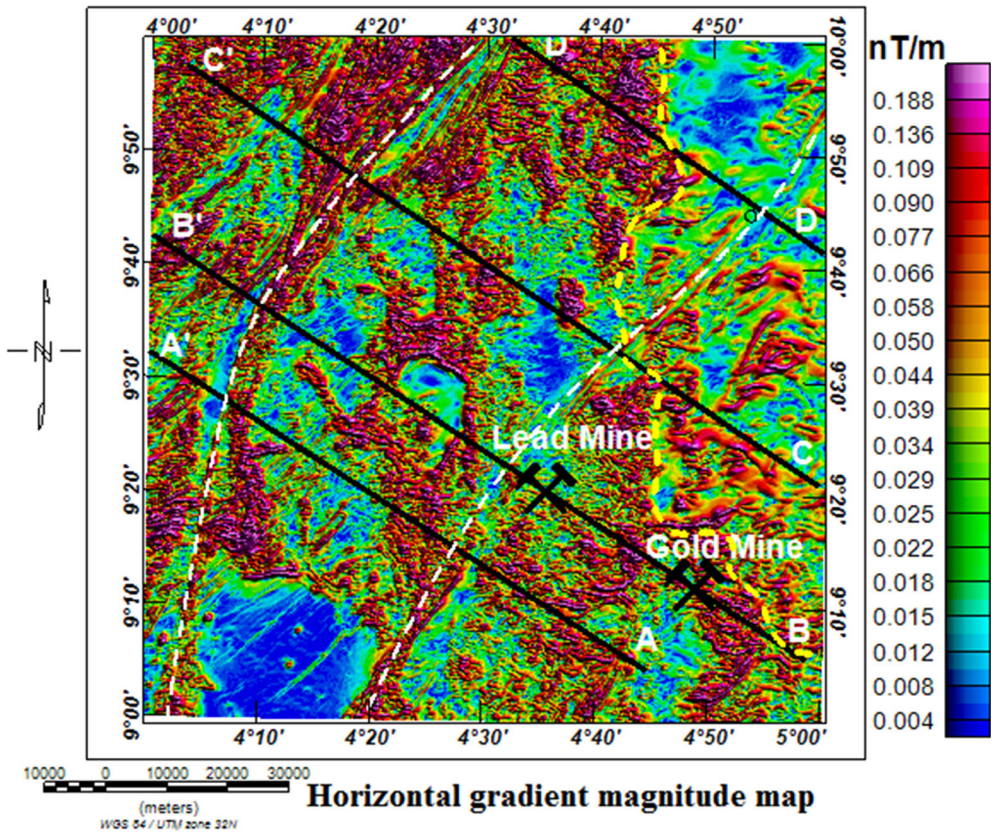

Figure 8
Colour-shaded horizontal gradient magnitude (HGM) map of the study area. The map highlights magnetic structures throughout the study area

show values ranging from high to low amplitudes. These explain why a shear zone is a zone of complex magnetic structures and geological bodies. The TGM interpretation, like FVD, highlights the widths of the shear zones at different locations. The shear zones are bounded by a high-amplitude magnetic anomaly in specific areas. The width of the shear zones is measured between successive crests. The various rock types identified around the zones include hornblende syenite, porphyroblastic gneiss, medium-grained schist, undifferentiated schist and many others.

5.3. *Horizontal Gradient Magnitude*

The HGM map (Fig. 8) was derived from the residual magnetic intensity map that has been reduced to the magnetic equator. The purpose is to correct the dependence of the method on the geomagnetic inclination and centre the HGM maxima on the edges of the causative bodies. The HGM interpretation highlights edges of magnetic structures and rocks in different parts of the study area. Notably, the HGM shows pockets of magnetic source bodies in some parts of the sedimentary basin. The strikes of the magnetic source bodies are revealed in the lineament map derived from the HGM anomaly map (Fig. 9). The predominant geological strikes of most magnetic source bodies in different parts of the study area are NE–SW, ENE–WSW and E–W respectively, while the shear zones exhibit mainly NNE–SSW geological strikes. The minor fractures spread throughout different parts of the study area. The younger rocks and a few minor faults have been identified as sites of important mineral deposits, especially the NE-trending ones. The gold deposits in the study area are concentrated in minor linear magnetic source bodies, while the lead deposits are

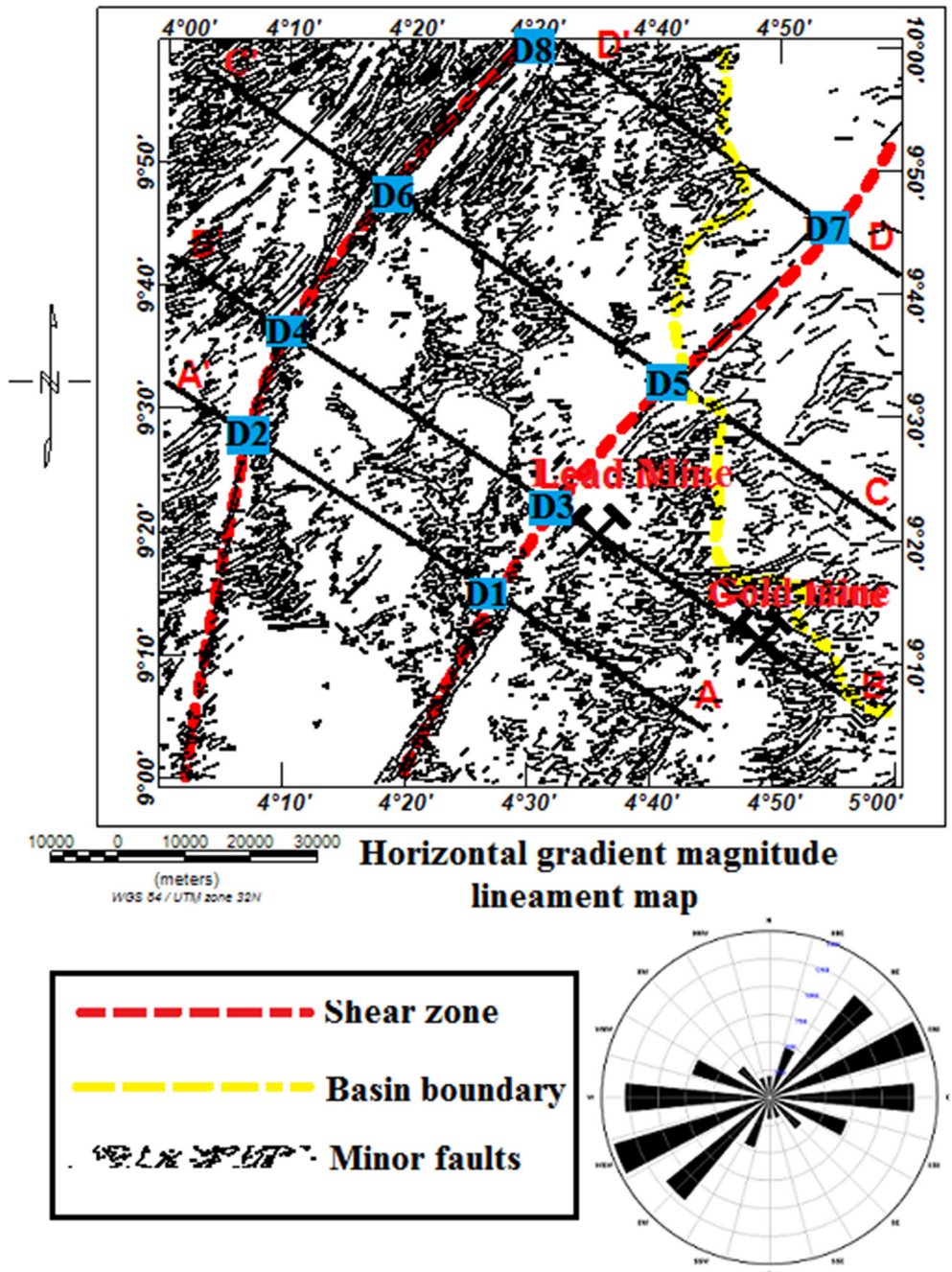

Figure 9
Lineament map derived from the HGM anomaly map. The map highlights the two major shear zones and minor faults throughout the study area. Parts of the major faults identified as D1, D2, D3, D4, D5, D6, D7 and D8 are points where the dip directions were determined

associated with younger volcanic rocks intruding the magnetic basement close to the shear zone in the eastern study area. To understand the dip direction of the shear zones and the associated minor faults, the offsets of the HGM maxima from the TGM maxima at different parts of the two shear zones through the

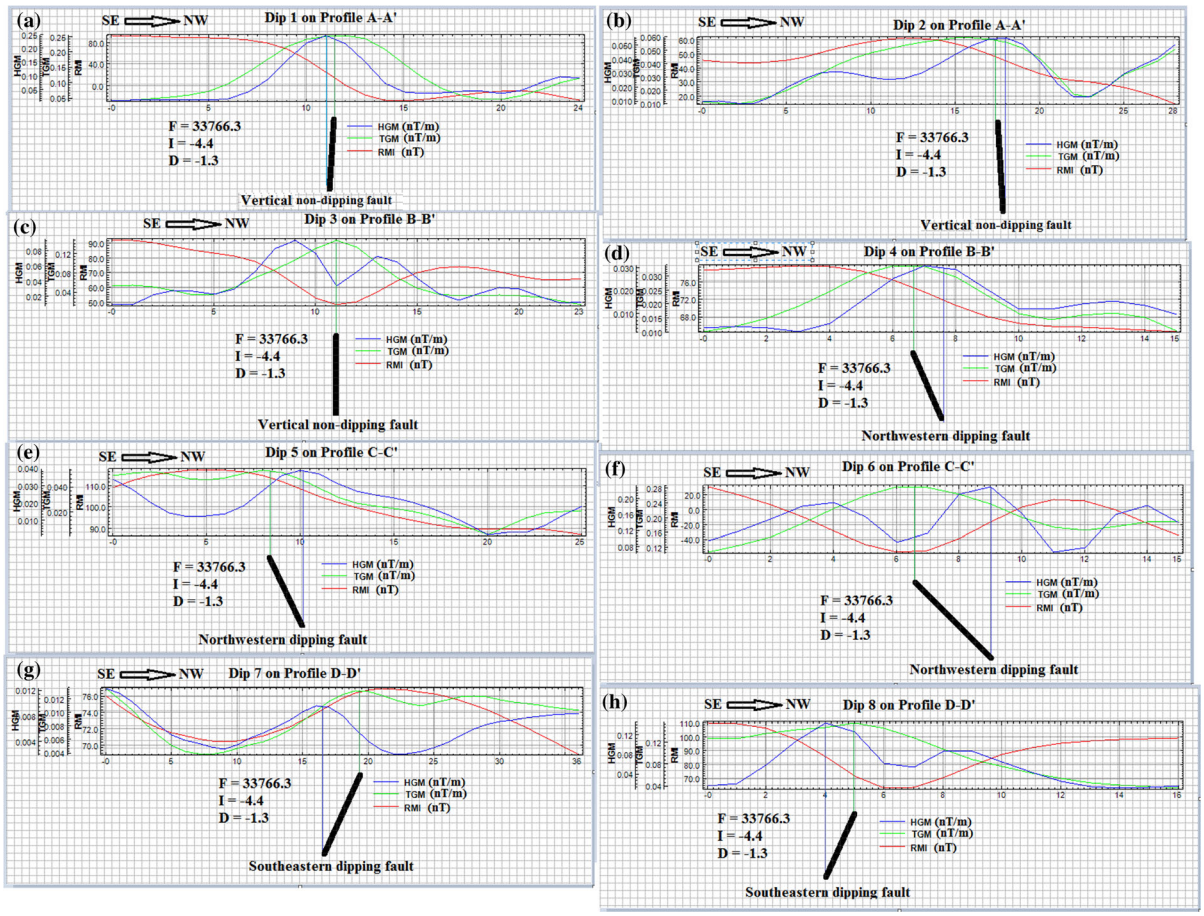

Figure 10

The dip directions obtained for various parts of the mega-structural shear zones are presented. The geomagnetic field, inclination and declination are 33,766.3 nT, –4.4° and –1.3°, respectively. Note that the maxima of the TGM may not necessarily coincide with the edges of the shear zones. **a** Vertical non-dipping contact D1 on the eastern shear zone in part of A–A′; **b** vertical non-dipping contact D2 on the western shear zone in part of A–A′; **c** vertical non-dipping contact D3 on the eastern shear zone in part of B–B′; **d** north-western-dipping contact D4 on the western shear zone in part of B–B′; **e** north-western-dipping contact D5 on the eastern shear zone in part of C–C′; **f** north-western-dipping contact D6 on the western shear zone in part of C–C′; **g** south-eastern-dipping contact D7 on the eastern shear zone in part of D–D′; **h** south-eastern-dipping contact D8 on the western shear zone in part of D–D′

study area were determined. The offsets of the HGM from the TGM give the approximate dip direction, while zero offsets represent vertical non-dipping contacts (Philip, 2000; Awoyemi, Ajama, et al., 2017). The parts identified as D1, D3, D5 and D7 in Fig. 9 are points on the shear zone through the eastern parts of the study area where the dip direction for the structure was determined, while the parts labelled D2, D4, D6 and D8 represent points on the shear zone through the western parts of the study area where the dip direction for the structure was also determined (Fig. 9). The results for each part are presented in Fig. 10. Three dipping contacts, namely, vertical non-dipping contact, north-western (NW) and south-eastern (SE)-dipping contacts, were identified on the shear zones through the area. The eastern shear zone exhibits mainly a vertical non-dipping contact (Fig. 10a, c). To the north, the eastern shear zone rotates clockwise and subsequently dips north-westerly (Fig. 10e). At the extreme north, the dip direction reversed to south-easterly (Figs. 10g). The western shear zone exhibits fairly the same dip directions as the eastern counterpart. The observed transformation in the dip directions from one part of

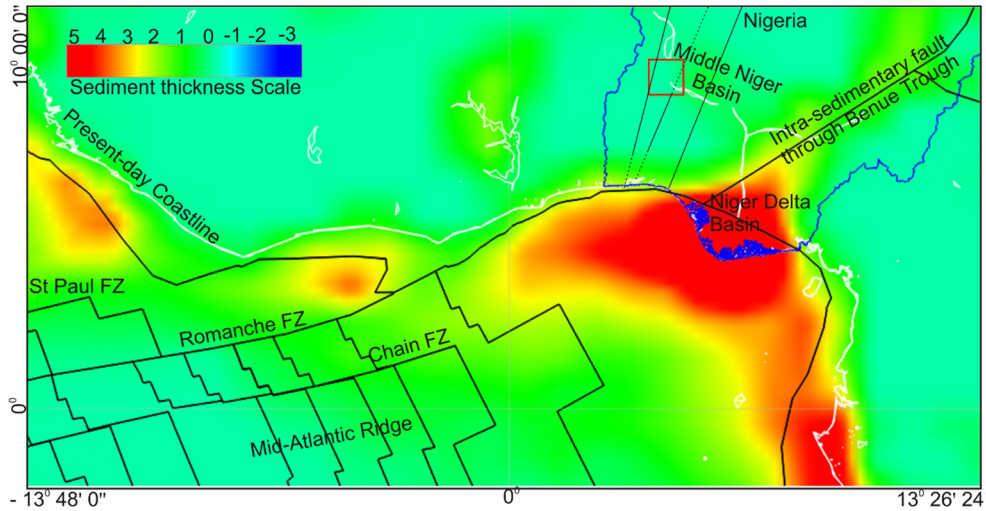

Figure 11

Map of the present-day crustal sedimentary thickness highlighting the coastlines (white lines), Saint Paul, Romanche and Chain fault zones (FZ) associated with the mid-Atlantic ridge system, the intra-sedimentary fault through the Nigeria Benue Trough and the two regional shear zones trespassing the study area. The study area is the red square outline. The two shear zones passing through the study area are shown. The Ifewara–Zungeru fault is to the east of the study area

the shear zones to another is a reflection of the dynamic nature of the Pan-African deformation that affected the area.

Figure 11 highlights the present-day crustal sedimentary thickness, the coastlines and the main oceanic transform faults, namely Saint Paul, Romanche and Chain fault zones associated with the mid-Atlantic ridge system (Müller et al., 2018; Seton et al., 2012). The map shows the study area and the shear zones in the Nigeria basement complex. The possible extension of the shear zones across the Dahomey Basin to link with the Romanche transform fault was highlighted on the map (Fig. 11). The middle Niger Basin appears to stem from the Benue Trough, even though both basins are structurally different. The basement faults and other overprinted structures provide evidence for the structural control of many economic mineral deposits in Nigeria. Unlike the Benue Trough, the middle Niger Basin is connected to a few regional faults crosscutting the basin at oblique angles (see Fig. 11).

5.4. Three-Dimensional Euler Deconvolution

The interpretation of the 3D Euler deconvolution was carried out using a structural index of 1.0. The choice of 1.0 structural index is to map younger volcanic intrusion along the shear zones and other parts of the crystalline basement and sedimentary terrain. The result obtained shows several parts of the crystalline basement to be underlain by younger volcanic rocks at very shallow depth (less than 300 m) (Fig. 12), though a small area at the centre of the study area shows magnetic source bodies at a depth greater than 1000 m. There are equally linear solutions coinciding with the shear zones and other minor faults. The solution of the 3D Euler deconvolution in the shear planes shows magnetic rocks at very shallow depth (mainly below 300 m). Similarly, the depth solutions for the magnetic bodies within the basin are from 300 m and above. Some magnetic source bodies within the basin have depths between 300 and 600 m and are attributed to shallow-seated younger volcanic rocks that are overprinted on the magnetic basement that failed to subside (Braide, 1992). The second category of magnetic source bodies have depths greater than 1000 m and indicate the deep-seated younger volcanic rocks that are overprinted on the subsided portion of the basement below a thick sedimentary layer. A drape map of Euler deconvolution and greyscale FVD interpretation (Fig. 13) highlights the shear zones, the minor

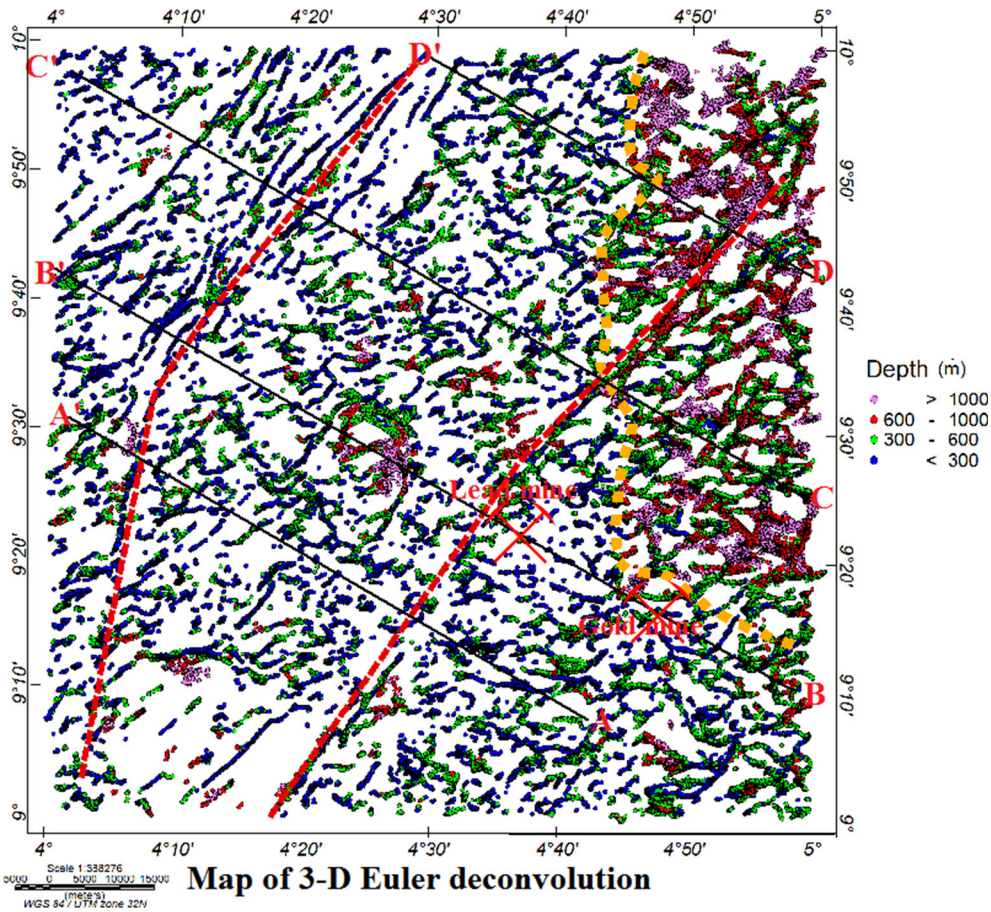

Figure 12
Solutions derived from Euler deconvolution interpretation for a structural index of 1.0. The map highlights magnetic lineaments and structures throughout the study area and specifically within the shear zones

faults and the adjoining sedimentary terrain of the middle Niger Basin. The shear zones show mainly NNE-trending geological strikes through the crystalline basement and the sedimentary basin.

5.5. Source Parameter Imaging

The depth distribution for the magnetic source bodies throughout the study area was studied using an SPI solution (Fig. 14). The result shows a very large portion of the crystalline formation to be underlain by shallow magnetic source bodies at extremely shallow depths (below 300 m), except for a small location at the centre of the study area. The middle Niger Basin shows a depth up to 1000 m and above. The SPI map equally highlights the boundaries of the shear zones. The presence of younger igneous intrusions and other similar crystalline rocks such as mylonites in the shear zones suggests possible sites of economic mineral deposits in the area.

5.6. Radiometric Ratio

The ratio of K/eTh was used to identify areas of preferential potassium enrichment (Boyle, 1979) (Fig. 15). This feature is seemingly notable in parts of the shear zones, especially the western shear zone where it appears as fairly broad linear structures. This feature is associated with the younger volcanic rock within the shear zones. Aside from the shear zones, the minor faults equally exhibit potassium

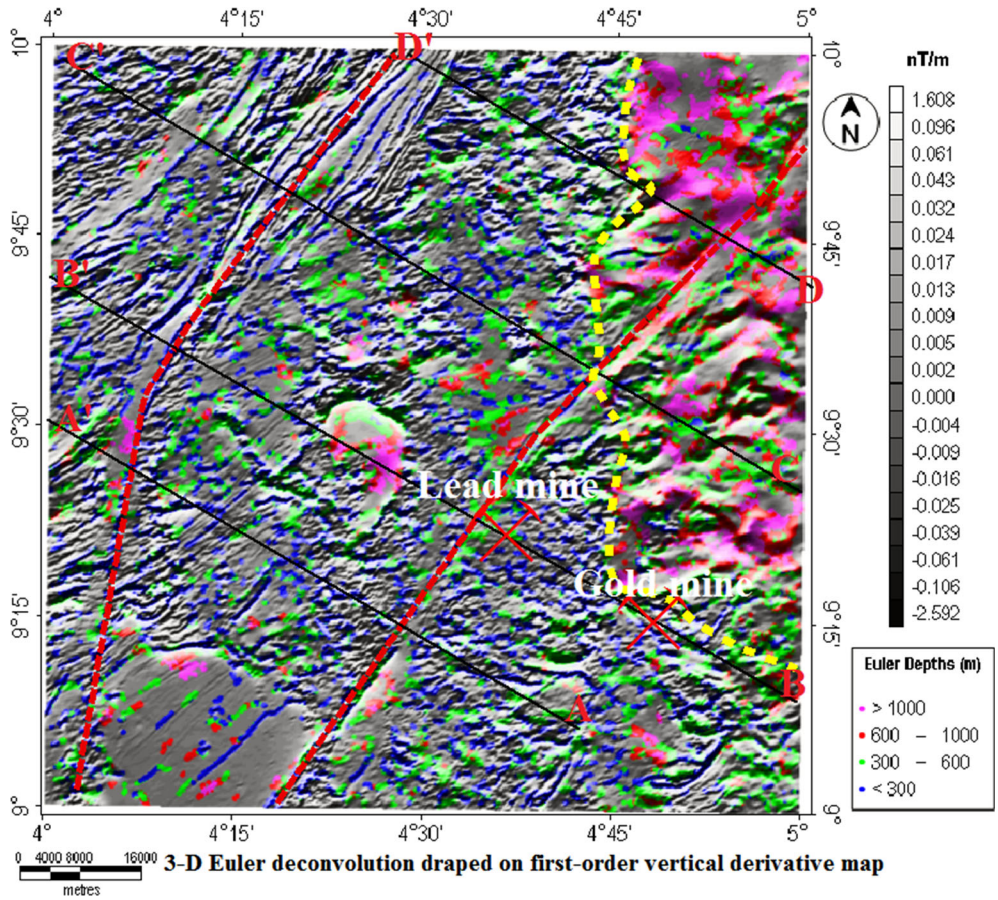

Figure 13
Map of 3D Euler deconvolution of a structural index of 1.0 draped over the greyscale first-order vertical derivative map. The map highlights magnetic lineaments and the adjoining sedimentary formations in the study area

enrichment in specific locations. The gold mine identified in a separate location in the study area is marked by high potassium concentration to low thorium concentration. These mineral signatures indicate that some minor faults and parts of the shear zones may be favourably rich in gold and other associated minerals. In addition, the young igneous rocks also display potassium enrichments, in most cases accompanied by high uranium and low thorium concentration. The transition zone between the middle Niger Basin, especially where the sedimentary formation directly interacts with the crystalline rocks, can be a good location for targeting mineral deposits such as gold, lead and copper. The contacts of the crystalline basement and the middle Niger Basin were precisely identified with the magnetic data (yellow broken outline). The boundary of the sedimentary basin indicated by the radiometric ratio map (Fig. 15) departs slightly from that indicated by the magnetic data (yellow broken line). This departure implies that the capability of radiometric data to precisely map geological contact is low. However, the radiometric data complement the magnetic data in identifying the transition zone which is the area between the magnetic and radiometric boundaries (Fig. 15).

5.7. *Ternary Radiometric Map of Potassium Concentration and its Ratios*

To visualize the abundance of potassium relative to thorium and uranium, the potassium concentration

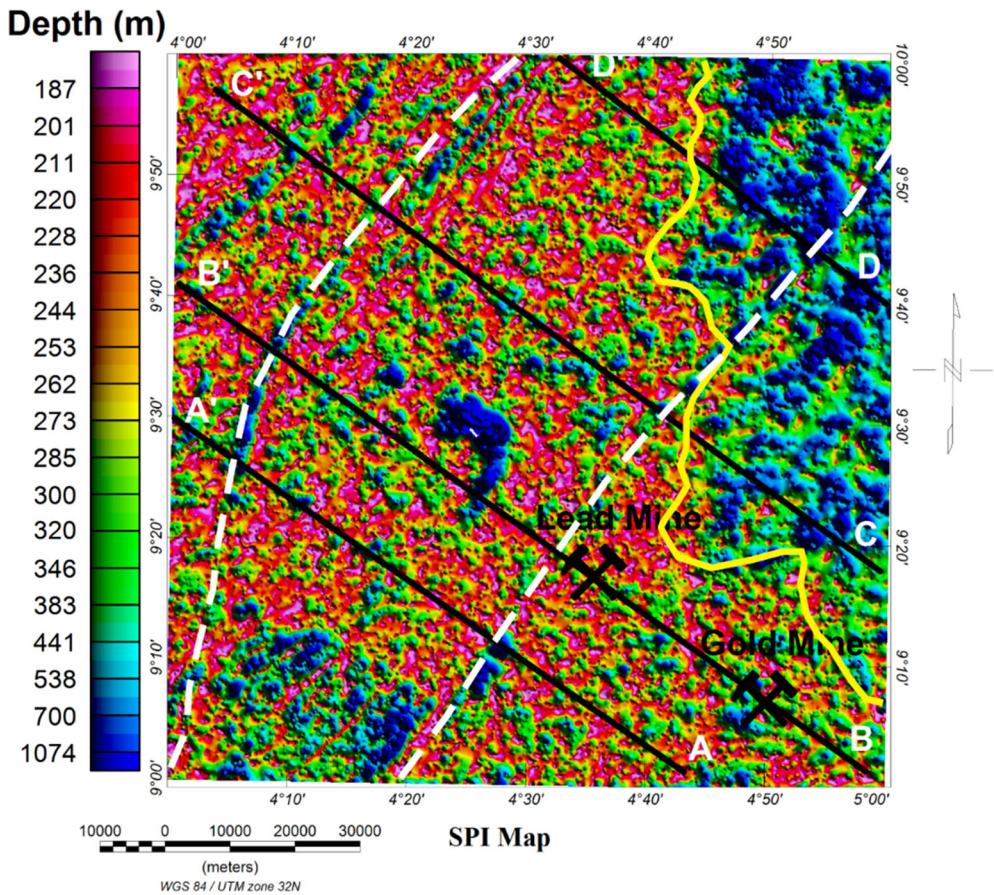

Figure 14
Colour-shaded map showing depth distribution for magnetic rock derived from SPI interpretation. The map highlights magnetic lineaments and the adjoining sedimentary formations in the study area

was assigned to red, while each of the ratios K/eTh and K/eU were assigned to green and blue colours, respectively, to form a ternary radiometric map (Dentith & Mudge, 2014). The regions where potassium is abundant and the other radio-elements are low appear white and where both radio-elements have high concentrations, the regions appear red. Where the concentration of both radio-elements is low, it appears black (Dentith & Mudge, 2014). The result obtained in Fig. 16 further justified potassium enrichment in areas previously identified. An overlay of minor lineaments shows high lineament density between the boundaries of many of the geological formations. The high lineament density zones helped identify the lithological boundaries, and also helped distinguish fractured, fairly fractured and non-fractured basement rocks. It equally helps identify the boundaries and widths of the shear zones traversing the study area. The boundary is highlighted by high lineament density, as the individual formation is distinguished by the radiometric colour variation.

5.8. *Two-Dimensional Subsurface Models of the 3D Solutions*

To understand the extent of the structural and lithological deformations in the present study area, four NW-trending 2D cross sections, A–A′, B–B′, C–C′ and D-D′, were used for subsurface

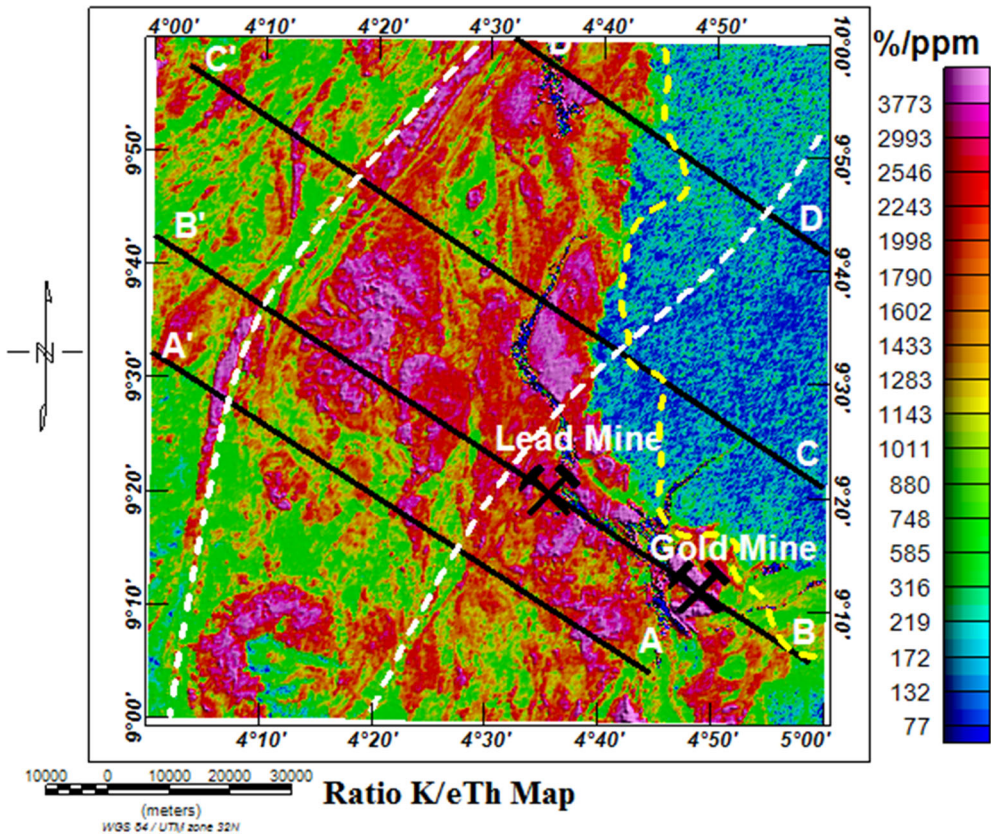

Figure 15
Colour-shaded map showing potassium enrichment for magnetic structures and rocks of tectonic origin derived from the K/Th ratio. The map highlights possible mineralized areas in the crystalline basement and the adjoining sedimentary basin

models of the 3D grids (see Figs. 12 and 14). The subsurface models were extracted from the SPI grid, while the Euler solution for each model was extracted from the 3D Euler grid using an in-house computer application (see Fig. 17a, b). The first two models through the cross sections A–A′ and B–B′ (Fig. 17a, b) within the crystalline basement show the magnetic basement (migmatite–gneiss complex) and the overprinted younger volcanic rocks at shallow depth. The volcanic rocks, in certain locations, can be distinguished from the outcropped metamorphic basement by their cross-cutting, discordant and steeply dipping altitude compared to the metamorphic basement which is generally a low-lying concordant crystalline rock (Pidgeon et al., 1976). The fresh basement, unlike the outcrop weathered basement, appeared to preserve many notable features of the Pan-African orogeny such as the basement deformations, geological strikes and dip of geological structures. The last two models through the cross sections C–C′ and D–D′, (Fig. 17c, d) highlight the basement topography in parts of the middle Niger Basin and the crystalline basement. The migmatite-gneiss basement underlying a significant portion of the middle Niger Basin rises and falls like crests and troughs in wave motion (see Fig. 17d). The upward and downward displacement of the basement is an indication that it has suffered intense fragmentation and subsidence that allowed sediments to accumulate. The depths to the tops of the basement or, more specifically, the sedimentary thicknesses, vary extensively. This is because the crystalline basement below the

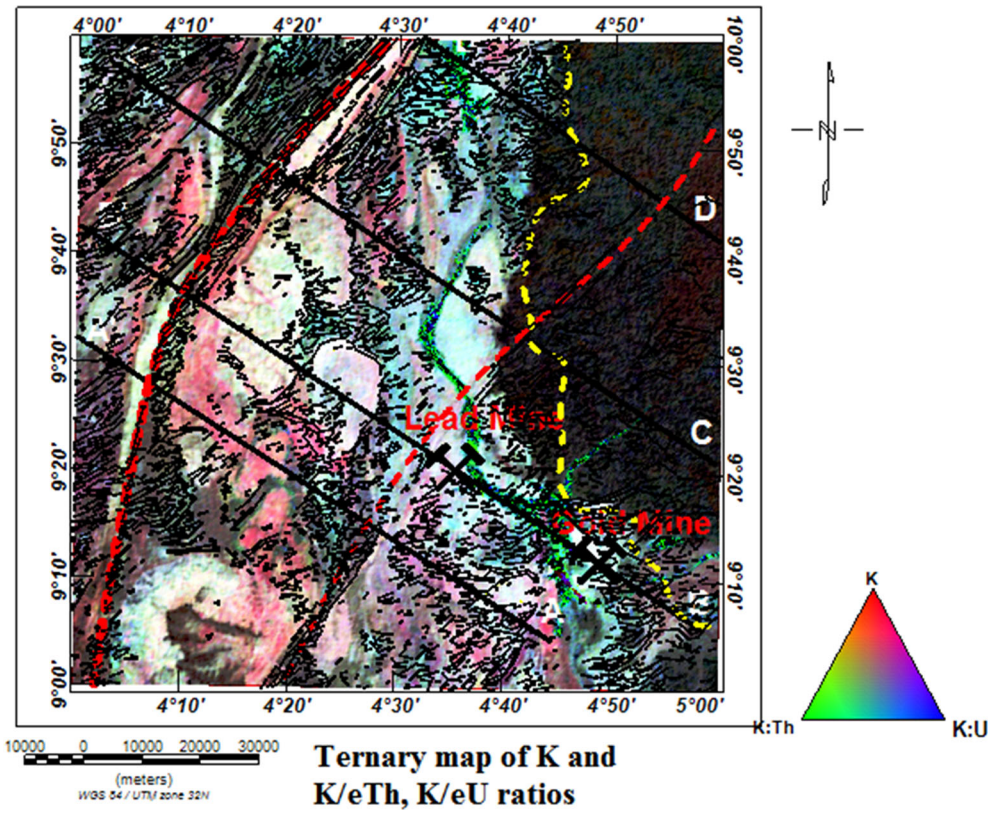

Figure 16
Map showing potassium enrichment for magnetic structures and rocks of tectonic origin derived from RGB ternary radiometric map of K, and ratios K/eTh and K/eU. The map highlights areas with potassium enrichment in the crystalline basement and the adjoining sedimentary basin

sedimentary sequences did not evenly subside. This, therefore, gives rise to shallow and deeper depths within the sedimentary basin. The depths to the top of the shallow basement can be less than 500 m in certain locations, while the depths to the top of the deeper basement can be up to 3000 m. The sedimentary thicknesses for the section covered in this study showed the possibility of a depth up to 3000 m in specific locations as the elevations of the sedimentary sequences were not ignored (Fig. 17d). Note that the activities that resulted in the basin fragmentation and subsidence were dated back to its evolution (Mullan, 1979). The middle Niger Basin, unlike the Benue Trough, did not have volcanic rocks within the sedimentary units (Kogbe, 1989; Rahaman et al., 2018). The observed magnetic anomalies in the sedimentary area come from the younger volcanic rocks that lie on and within the magnetic basement. There is also the presence of ironstones in the sedimentary terrane of the study area. The wavelengths of the magnetic field emanating from such materials are far too short compared to the magnetic field emanating from the deeper and highly magnetic intrusions within the basement.

6. Conclusion

The study of the earth's magnetic structures in this study shows possible ways to characterize crustal structures for understanding its tectonic and structural frameworks. The airborne magnetic and radiometric data of the studied area identified linear geological structures which include but are not

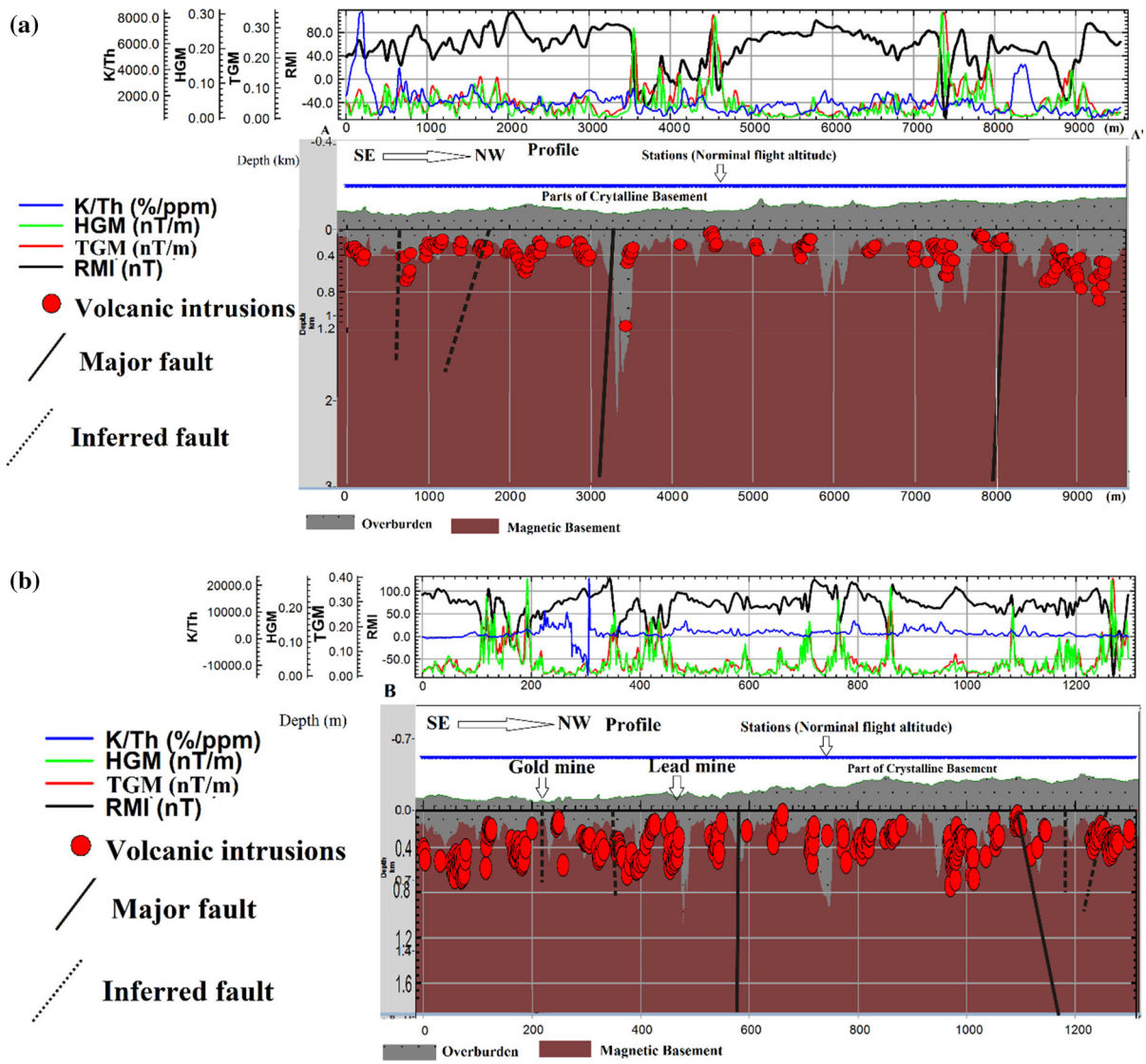

Figure 17

Two-dimentional (2D) depth distribution for the magnetic basement and the overprinted younger volcanic rocks derived from the SPI and the 3D Euler deconvolution method respectively on the line cross-section through **a** A–A′. **b** B–B′. **c** C–C′. **d** D–D′. The maps show the positions and dips of important faults in the crystalline basement of the study area

limited to faults, joints and shear zones. We identified several igneous rocks within the metamorphic basement underlying a significant portion of the middle Niger Basin, the crystalline basement terrane and parts of the shear zones. The igneous intrusions in both the crystalline basement and the sedimentary terrain provide evidence for the tectono-thermal stress regime during the Pan-African orogeny that resulted in major structural deformation and compositional differentiation of the Archaean basement. We equally identified linear magnetic highs and a few linear narrow magnetic lows marked by a high potassium-to-thorium ratio, indicating possible hydrothermal alteration. This feature is recognized as the main minerals signatures responsible for the gold mineralization in parts of the study area and may be

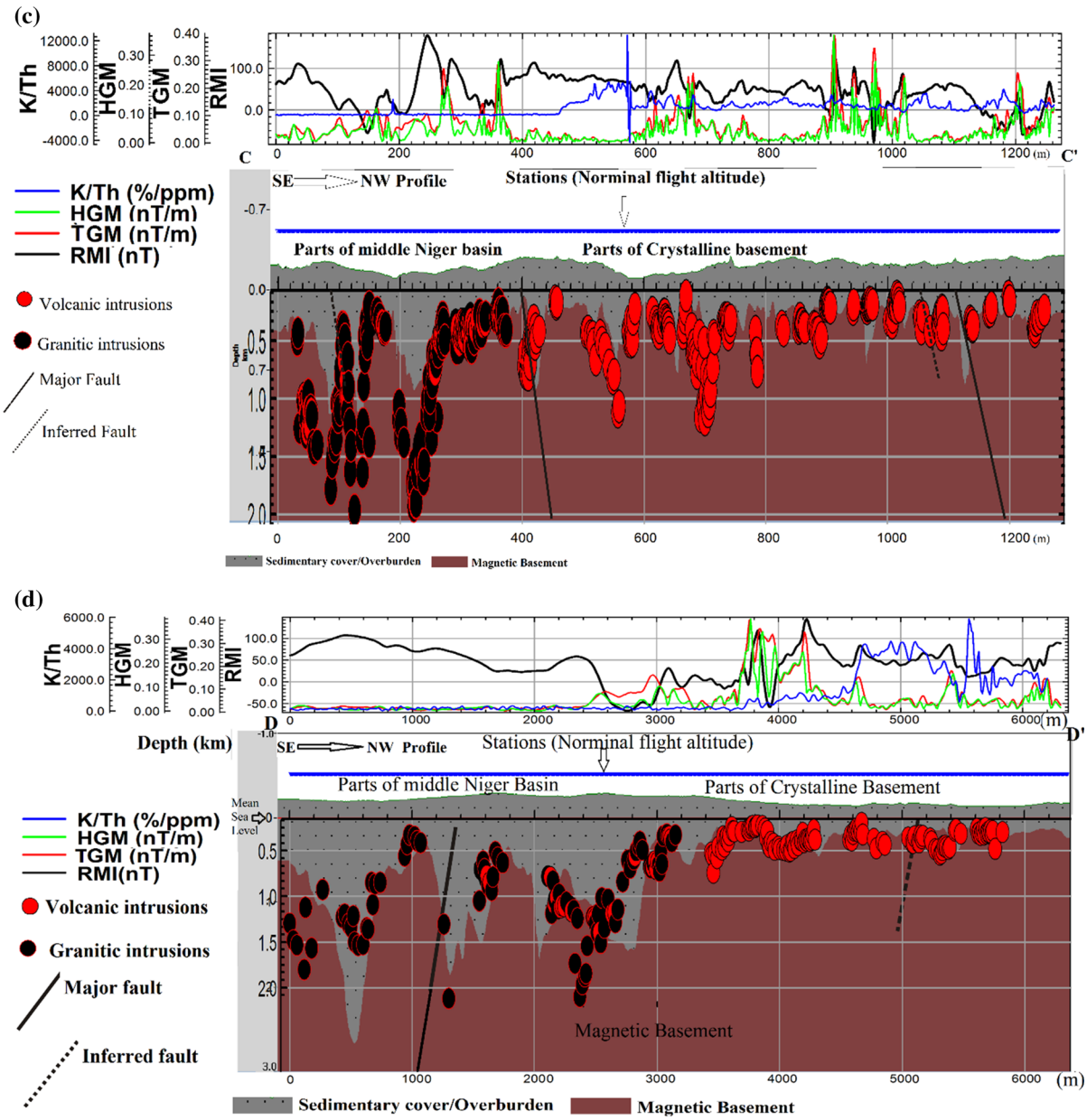

Figure 17
continued

used to guide the exploration gold in other parts of the studied area. A good number of the structures identified in the studied area exhibit NE–SW, ENE–WSW and E–W geological strikes. The depth variation for tectonic structures and igneous intrusions within the crystalline basement is between 180 and 300 m and up to 3000 m in the sedimentary terrain. The transition zone between the crystalline basement and the sedimentary terrain exhibits basement depths that are far less than those of the basin but slightly greater than the crystalline basement.

Acknowledgements

The authors appreciate Ibraj Mining and the West African Geo-mining Systems for granting access to the mining sites and for providing technical support for the study.

Funding

The authors have not disclosed any funding.

Declaration

Conflict of interest The authors declare that they have no known competing financial interests or personal relationships that could have appeared to influence the work reported in this paper.

Publisher's Note Springer Nature remains neutral with regard to jurisdictional claims in published maps and institutional affiliations.

References

Adebiyi, L. S., Eluwole, A. B., Fajana, A. O., Salawu, N. B., Falade, S. C., Dopamu, K. O., & Alejolowo, E. A. (2021). Integrated geophysical methods for delineating crustal structures and hydrothermal alteration zones for mineral exploration projects in parts of west-central Nigeria. *Modeling Earth Systems and Environment*. https://doi.org/10.1007/s40808-021-01275-5

Adebiyi, L. S., Fatoba, J. O., Salawu, N. B., Dopamu, K. O., Abdulraheem, T. Y., Obaseki, O. S., Olasunkanmi, N. K., & Adediran, S. O. (2020). Analysis of aeromagnetic data: Application to Early – Late Cretaceous events in parts of Lower Benue trough, Southern Nigeria. *Journal of Applied Geophysics, 178*, 1–18.

Adeniyi, J. O. (1985). Ground total magnetic intensity in part of Nupe Basin and the adjacent Basement complex, Niger State, Nigeria. *Journal of Applied Science, 3*, 67–68.

Adepelumi, A. A., Ako, B. D., Ajayi, T. R., Olorunfemi, A. O., Awoyemi, M. O., & Falebita, D. E. (2008). Integrated geophysical studies of the Ifewara transcurrent fault system, Nigeria. *Journal of African Earth Science, 52*, 161–166.

Ajibade, A. C. (1988). Structural and tectonic evolution of the Nigerian basement with special reference to NW Nigeria. In *International Conference on Proterozoic geology and tectonics of high-grade terrain, University of Ile-Ife, Nigeria*.

Ajibade, A. C., Woakes, M., & Rahaman, M. A. (1987). Proterozoic crustal development in the Pan-African regime of Nigeria. In A. Kröner (Ed.), *Proterozoic lithospheric evolution* (pp. 259–271). American Geophysical Union.

Ajibade, A. C., & Wright, J. B. (1988). Structural relationships in the schist belts of northwestern Nigeria. In P. O. Oluyide (Ed.), *Precambrian Geology of Nigeria* (pp. 103–109). Geological Survey of Nigeria Publication.

Akingboye A. S., Ogunleye A. C., (2018). *Basement classification through enhanced magnetic data reductions in parts of Ekiti State, southwestern Nigeria - Scientific Figure on ResearchGate*. Available from: https://www.researchgate.net/figure/Contoured-Reduction-to-Magnetic-Equator-RTE-Map_fig2_321341385. Accessed 23 May 2021

Alessio, L., Cedric, T., Fred, B., Sierd, C., & Stuart, C. (2017). Lithosphere erosion and continental breaking. *Earth and Planetary Science Letters, 467*, 89–98.

Anifowose, A. Y. B., Oladapo, M. I., Akpan, O. U., Ologun, C. O., Adeoye-Oladapo, O. O., Tsebeje, S. Y., & Yabuku, T. A. (2010). Systematic Multi-technique Mapping of the Southern Flank of Iwaraja Fault, Nigeria. *Journal of Applied Science Technology, 15*(1–2), 70–76.

Awoyemi, M. O., Ajama, O. D., Hammed, O. S., Arogundade, A. B., & Falade, S. C. (2017). Geophysical mapping of buried faults in part of Bida Basin North Central Nigeria. *Geophysical Prospecting, 66*(1), 49–54.

Awoyemi, M. O., Hammed, O. S., Falade, S. C., Arogundade, A. B., Ajama, O. D., Iwalehin, P. O., & Olurin, O. T. (2017). Geophysical investigation of the possible extension of Ifewara fault zone beyond Ilesa area, southwestern Nigeria. *Arabian Journal of Geosciences, 10*(27), 1–14.

Bassey, E. E., Barth, N. E., Mohssen, M., & Monir, M. (2008). P-T conditions of Pan-African orogeny in southeastern Nigeria. *Central European Geology., 51*(4), 359–378.

Boyle, R. W. (1979). The geochemistry of gold and its deposits. *Geological Survey of Canada Bulletin, 280*, 584p.

Braide, S. P. (1992). Geological development, origin and energy mineral resources potential of the Lokoja Formation in the southern Bida Basin. *Journal of Mining and Geology, 28*, 33–44.

Brigs, I. C. (1974). Machine contouring using minimum curvature. *Geophysics, 39*(1), 39–48.

Cordell, L., Grauch V.J.S., (1982). Mapping basement magnetization zones from aeromagnetic data in the San Juan Basin, New Mexico: 52nd Annual International Meeting, SEG, Expanded Abstracts, 246–247

Dada, S.S., (2008). *Proterozoic evolution of the Nigeria–Boborema province*. In: Pankhurst, R.J., RAJ, Trouw, de Brito Neves, B.B., de Wit, M.J. (Eds.), West Gondwana: precenozoic correlations across the south Atlantic region. 294. Geological Society, London, pp. 121–136. https://doi.org/10.1144/sp294.7. Special Publications.

Dada, S. S. (1998). Crust-forming ages and Proterozoic crustal evolution in Nigeria: A reappraisal of current interpretations. *Precambrian Research, 87*, 65–74.

Dada, S. S., Tubosun, I. A., Lancelot, J. R., & Lau, A. U. (1993). Late Archaean U-Pb age for the reactivated basements of northeastern Nigeria. *Journal of African Earth Sciences (and the Middle East), 16*, 405–412.

Dentith, M., Mudge, S. (2014). *Geophysics for the mineral exploration geoscientist*. AusIMM Bulletin, Australasian Institute of Mining and Metallurgy. https://doi.org/10.1017/cbo9781139024358

Ball, E. (1980). An example of very consistent brittle deformation over a wide intracontinental area: The late Pan-African fracture system of the Tuareg and Nigerian shield. *Tectonophysics*, *61*(4), 363–379. https://doi.org/10.1016/0040-1951(80)90240-1.

Fedi, M., & Florio, G. (2001). Detection of potential fields source boundaries by the enhanced horizontal derivative method. *Geophysical Prospecting, 49*, 40–58.

Ferré, E., Gleizes, G., Bouchez, J. L., & Nnabo, P. N. (1995). Internal fabric and strike-slip emplacement of the Pan-African granite of the Solli Hills, northern Nigeria. *Tectonics, 1*(4), 1205–1219.

Fitches, W. R., Ajibade, A. C., Egbuniwe, I. G., Holt, R. W., & Wright, J. B. (1985). Late Proterozoic schist belts and plutonism in NW Nigeria. *Journal of the Geological Society, 142*, 319–337.

Garba, I. (2000). Gold prospect of the Nigerian Pan-African terrain of West Africa. *Journal of Mining and Geology, 36*, 123–156.

Grant, N. K. (1969). The late precambrian to early paleozoic Pan-African Orogeny in Ghana, Togo, Dahomey, and Nigeria. *Geological Society of America Bulletin, 80*, 45–56.

Grant, N. K. (1978). Structural distinction between a metasedimentary cover and underlying basement in 600 M.Y. old Pan-African domain of northwestern Nigeria, West Africa. *Geological Society of America Bulletin, 89*, 50–58.

Gunn, P. J., Maidment, D., & Milligan., P.R. (1997). Interpreting aeromagnetic data in areas of limited outcrop. *Journal of Australian Geology & Geophysics, 17*(2), 175–185.

Hafeez, T. H. A., Youssef, M. A. S., & Mohamed, W. H. (2015). Utilization of airborne gamma ray spectrometric data for geological mapping and radioactive mineral exploration of Gabel Umm Tineidba area, south eastern desert, Egypt. *World Journal of Engineering, 12*, 149–160. https://doi.org/10.1260/1708-5284.12.2.149

Haruna, I. V. (2017). Review of the basement geology and mineral belts of Nigeria. *Journal of Applied Geology and Geophysics, 5*(1), 37–45.

Huang, L., & Guan, Z. (1998). Discussion on "magnetic interpretation using the 3-D analytic signal" by Roest W.R., Verhoef J. and Pilkington M. *Geophysics, 63*, 667–670.

Kogbe, C. A. (1981). Geological Interpretation of Landsat Imagery of part of Central Nigeria. *Journal of Mining and Geology, 28*, 66–69.

Kogbe, C.A., (1989). Cretaceous and tertiary of the iullemmeden basin in Nigeria. In: Kogbe, C.A. (Ed.), Geology of Nigeria, 2nd edition. pp. 377–421.

Kogbe, C. A., Ajakaiye, D. E., & Matheis, G. (1983). Confirmation of rift structure along the middleNiger Valley, Nigeria. *Journal of African Earth Sciences, 1*, 127–131.

Kröner, A., Ekwueme, B. N., & Pidgeon, R. T. (2001). The oldest rocks in West Africa: SHRIMP zircon age for early Archaean migmatitic orthogneiss at Kaduna, Northern Nigeria. *The Journal of Geology, 109*, 399–406.

Li, X. (2006). Understanding 3-D analytic signal amplitude. *Geophysics, 71*, 13–16. https://doi.org/10.1190/1.2184367

MacLeod, L. N., Jones, K., & Dai, T. F. (1993). 3-D analytic signal in the interpretation of total magnetic field data at low magnetic latitudes. *Exploration Geophysics, 24*, 679–688.

Mccurry, P., & Wright, J. B. (1977). Geochemistry of calc-alkaline volcanics in northwestern Nigeria, and a possible Pan-African suture zone. *Earth and Planetary Science Letters, 37*, 90–96.

Megwara, J. U., & Udensi, E. E. (2014). Structural analysis using aeromagnetic data: Case study of parts of Southern Bida Basin, Nigeria and the surrounding basement rocks. *Earth Science Research, 3*(2), 27–42.

Misra, K.C., (2000). *Understanding mineral deposits*. Springer-Science + Business Media, B.V. ebook, Vol. 1.

Moritz, M., (2009). *Magnetic anomaly interpretation of the North German Basin: Results from depth estimation and 2D-modeling*. Bachelor of Science Thesis, Department of Earth & Space Sciences, Jacobs University Bremen, Bremen, Germany.

Mullan, H. S. (1979). Structural distinction between a metasedimentary cover and an underlying basement in the 600 m.y. old Pan-African domain of northwestern Nigeria, West Africa. *Geological Society of America Bulletin, 90*, 983–984.

Müller, R. D., Cannon, J., Qin, X., Watson, R. J., Gurnis, M., Williams, S., et al. (2018). GPlates: Building a virtual Earth through deep time. *Geochemistry, Geophysics, Geosystems*. https://doi.org/10.1029/2018GC007584

Nabighian, M. N. (1972). The Analytic Signal of two-dimensional Magnetic Bodies with polygonal cross-section: Its properties and use for automated anomaly interpretation. *Geophysics, 37*(3), 507–517.

Nabighian, M. N., Grauch, V. J. S., Hansen, R. O., LaFehr, T. R., Li, Y., Peirce, J. W., Phillips, J. D., & Ruder, M. E. (2005). The historical development of the magnetic method in exploration. *Geophysics, 70*(6), 33–61.

Nigerian Geological Survey Agency, (2006a). Nationwide Geological Map. NGSA, 31 Shetima Munguno Crescent, Utako, Abuja, Nigeria.

Nigerian Geological Survey Agency, (2006b). Nationwide Aeromagnetic and Aeroradiometric Data. NGSA, 31 Shetima Munguno Crescent, Utako, Abuja, Nigeria.

Obaje, N.G., 2009. Geology and Mineral Resources of Nigeria". Lecture Notes in Earth Sciences: Springer Dordrecht Heidelberg London New York.

Odeyemi, I.B., 1976. Preliminary report on the field relationships of the basement complex rocks around Igarra Mid-West. (ed. Kogbe, C. A.) 59 – 63 (Elizabethan Press Lagos).

Odeyemi, I. B., Anifowose, A. Y. B., & Asiwaju-Bello, Y. A. (1999). Multitechnique graphical analysis of fractures from remote sensing images of basement regions of Nigeria. *J Mining Geol, 35*(1), 9–21.

Ohioma, J. O., Ezomo, F. O., & Akinsunmade, A. (2017). Delineation of Hydrothermally Altered Zones that Favour Gold Mineralization in Isanlu Area, Nigeria Using Aeroradiomatric Data. *International Annals of Science., 2*(1), 20–27.

Ojo, S. B., 1984. Middle Niger Basin Revisited, Magnetic constraints on gravity interpretations. Nigerian Mining and Geosciences Society Conference, Nsukka, Nigeria, Abstract vol., 52-53.

Ojo, S. B., Ajakaiye, D. E., 1989. Preliminary interpretation of gravity measurement in the middle Niger Basin area, Nigeria. In; C.A. Kogbe (editor), Geology of Nigeria, 2nd Edition, Elizabeth Publishing Co., Lagos., 347–358.

Ojo, S. B., 1990. Origin of a major magnetic anomaly in the Middle Niger Basin, Nigeria. *Tectonophysics, 85*, 153-162. dx.doi.org/https://doi.org/10.1016/0040-1951(90)90410-A.

Olaniyan, O., Abbah, U., Nwonye, N., Alichi, A. and Udensi, E.E., 2012. Interpretation of Total Magnetic Intensity Field over Bida Basin. Nigerian Geological Survey Agency. *Occasional Paper* No. 15. 98p.

Oluyide, P.O., 1988. Structural trends in the Nigerian basement complex. (ed). Oluyide, P. O.). 93 – 98 (Nigeria Geological Survey).

Phillips, J.D., 2000. Locating magnetic contacts: a comparison of the horizontal gradient, analytic signal, and local wavenumber methods. 70th Meeting, Calgary, *Society of Exploration*

Geophysicists, Expanded Abstracts with Biographies, 2000 Technical Program*,* 1, 402–405.

Pidgeon, R.T., Van Breemen, O., Oyawoye, M. O., 1976. Pan-African and earlier events in the basement complex of Nigeria. 25th Int. Geo. Congr. Sydney, Australia (Abstract Volume), 667.

Rahaman, M.A., 1976. Review of the Basement geology of southwestern Nigeria. – In: (ed. Kogbe, C. A) 41 – 58 (Elizabethan).

Rahaman, M. A. O., Fadiya, S. L., Adekola, S. A., Coker, S. J., Bale, R. B., Olawoki, O. A., Omada, I. J., Obaje, N. G., Akinsanpe, O. T., Ojo, G. A., & Akande, W. G. (2018). A revised stratigraphy of the Bida Basin Nigeria. *Journal of African Earth Science*. https://doi.org/10.1016/j.jafrearsci.2018.11.016

Rahaman, M. A., Ukpong, E. E., & Azmatullah, M. (1981). Geology of parts of Oban massif, southeastern Nigeria. *J. Min. Geo., 18*(1), 60–65.

Reid, A. B., Allsop, J. M., Granser, H., Millett, A. J., & Somerton, I. W. (1990). Magnetic interpretation in three dimensions using Euler deconvolution. *Geophy., 55*(1), 80–91.

Reid, A. B., Ebbing, J., Webb, S. J., 2011. Comment on 'A crustal thickness map of Africa derived from a global gravity field model using Euler deconvolution' by Getachew E. Tedla, M. van der Meijde, A. A. Nyblade and F. D. van derMeer, Geophy. J. Intern. **189** (3), 1217 – 1222.

Salawu, N. B., Fatoba, J. O., Adebiyi, L. S., Ajadi, J., Saleh, A., & Dada, S. S. (2020). Aeromagnetic and remote sensing evidence for the structural framework of the middle Niger and Sokoto basins, Nigeria. *Physics of the Earth and Planetary Interiors*. https://doi.org/10.1016/j.pepi.2020.106593

Salawu, N. S., Olatunji, S., Adebiyi, L. S., Olasunkanmi, N., & Dada, S. S. (2019). Edge detection and magnetic basement depth of Danko area, northwest Nigeria from low-latitude aeromagnetic anomaly data. *Springer Nature Journal., 1*, 1–16.

Salawu, N. B., Orosun, M. M., Adebiyi, L. S., & Abdulraheem, T. Y. (2020). Existence of subsurface structures from aeromagnetic data interpretation of the crustal architecture around Ibi, Middle Benue. *Nigeria. Springer Nature Journal., 2*, 1–11.

Seton, M., Müller, R. D., Zahirovic, S., Gaina, C., Torsvik, T., Shephard, G., Talsma, A., & Chandler, M. (2012). Global continental and ocean basin reconstructions since 200Ma. *Earth-Science Reviews, 113*(3), 212–270.

Shives, R., Charbonneau, B., & Ford, K. (2000). The detection of potassic alteration by gamma-ray spectrometry-recognition of alteration related to mineralization. *Geophysics-Wisconsin the Tulsa-Society of Exploration Geophysicists., 65*(6), 2001–2011.

Thieblemont, D. (Ed.) (2016) Geological map of African at 1: 10M scale. CGMW-BRGM (edit) et al.

Thompson, D. T. (1982). EULDPH: A new technique for making computer-assisted depth estimates from magnetic data. *Geophysics, 47*(1), 31–37.

Thurston, J. B., & Smith, R. S. (1997a). Automatic conversion of magnetic data to depth, dip, and susceptibility contrast using the SPI method. *Geophysics, 62*(3), 807–813.

Thurston, J. B., & Smith, R. S. (1997b). Automatic conversion of magnetic data to depth, dip, and susceptibility contrast using the SPITM method. *Geophysics, 62*(3), 807–813.

Udensi, E.E. (2001). *Interpretation of the total magnetic field over the Nupe basin in West Central Nigeria using aeromagnetic data*. PhD thesis Department of Physics ABU, Zaria, Nigeria

Udensi, E. E., & Osasuwa, I. B. (2004). Spectra determination of depths to magnetic rocks under the Nupe Basin, Nigeria. *Nigeria Association of Petroleum Explorationists Bulletin, 17*, 22–37.

Udensi, E. E., Osazuwa, I. B., & Daniyan, M. A. (2003). Trend analysis of the total magnetic field over the Bida Basin, Nigeria. *Nigerian Journal of Physics, 15*, 143–151.

USGS. (2017). *Shuttle radar topography mission, 1 Arc second scene, filled-finished-B, global land cover facility*. College Park: University of Maryland.

Verduzco, B., Fairhead, J. D., Green, C. M., & Mackenzie, C. (2004). New insights into magnetic derivatives for structural mapping. *The Leading Edge., 23*, 116–119.

Whiteman, A. (1982). *Nigeria: Its petroleum geology, resources and potential*. Vol. 1 and 2, Graham and Trotman, London, 349.

Wright, J. B., Hastings, D. A., Jones, W. B., & Williams, H. R. (1985). *Geology and mineral resources of West Africa*. https://doi.org/10.1016/0899-5362(87)90065-0